

On the role of ground state correlations in hypernuclear non–mesonic weak decay

E. Bauer^{1,2*} and G. Garbarino³

¹*Departamento de Física, Universidad Nacional de La Plata,
C. C. 67, 1900 La Plata, Argentina*

²*Instituto de Física La Plata, CONICET, 1900 La Plata, Argentina*

³*Dipartimento di Fisica Teorica, Università di Torino, I-10125 Torino, Italy*

(Dated: May 8, 2018)

Abstract

The contribution of ground state correlations (GSC) to the non–mesonic weak decay of ${}_{\Lambda}^{12}\text{C}$ and other medium to heavy hypernuclei is studied within a nuclear matter formalism implemented in a local density approximation. We adopt a weak transition potential including the exchange of the complete octets of pseudoscalar and vector mesons as well as a residual strong interaction modeled on the Bonn potential. Leading GSC contributions, at first order in the residual strong interaction, are introduced on the same footing for all isospin channels of one– and two–nucleon induced decays. Together with fermion antisymmetrization, GSC turn out to be important for an accurate determination of the decay widths. Besides opening the two–nucleon stimulated decay channels, for ${}_{\Lambda}^{12}\text{C}$ GSC are responsible for 14% of the rate Γ_1 while increasing the Γ_n/Γ_p ratio by 4%. Our final results for ${}_{\Lambda}^{12}\text{C}$ are: $\Gamma_{\text{NM}} = 0.98$, $\Gamma_n/\Gamma_p = 0.34$ and $\Gamma_2/\Gamma_{\text{NM}} = 0.26$. The saturation property of Γ_{NM} with increasing hypernuclear mass number is clearly observed. The agreement with data of our predictions for Γ_{NM} , Γ_n/Γ_p and Γ_2 is rather good.

PACS numbers: 21.80.+a, 25.80.Pw.

*Electronic address: bauer@fisica.unlp.edu.ar

I. INTRODUCTION

The study of nuclear systems with strangeness is a relevant question in modern nuclear and hadronic physics [1], which also implies important links with astrophysical processes and observables as well as with QCD, the underlying theory of strong interactions. Various strange nuclear systems can be studied in the laboratory, ranging from hypernuclei and kaonic nuclei to exotic hadronic states such as strangelets, H -dibaryons and pentaquark baryons. Strangeness production can also be investigated in relativistic heavy-ion collision experiments, whose main aim is to establish the existence of a quark-gluon plasma. Moreover, the cold and dense matter contained in neutron stars is expected to be composed by strange hadrons, in the form of hyperons and Bose-Einstein condensates of kaons, and eventually by strange quark matter for sufficiently dense systems.

The existence of hypernuclei —bound systems of non-strange and strange baryons— opens up the possibility to study the hyperon-nucleon and hyperon-hyperon interactions in both the strong and weak sectors. In turn, such interactions are important inputs, for instance, when investigating the macroscopic properties (masses and radii) of neutron stars. The best studied hypernuclei contain a single Λ -hyperon. In a nucleus the Λ can decay by emitting a nucleon and a pion (mesonic mode) as it happens in free space, but its (weak) interaction with the nucleons opens new channels which are indicated as non-mesonic decay modes (for recent reviews see Refs. [2–6]). These are the dominant decay channels of medium-heavy nuclei, where, on the contrary, the mesonic decay is disfavoured by the Pauli blocking effect on the outgoing nucleon. In particular, one can distinguish between one- and two-body induced decays, $\Lambda N \rightarrow nN$ and $\Lambda NN \rightarrow nNN$. The hypernuclear lifetime is given in terms of the mesonic ($\Gamma_M = \Gamma_{\pi^-} + \Gamma_{\pi^0}$) and non-mesonic decay widths ($\Gamma_{NM} = \Gamma_1 + \Gamma_2$) by $\tau = \hbar/\Gamma_T = \hbar/[\Gamma_M + \Gamma_{NM}]$. The various isospin channels contribute to the one- and two-nucleon induced non-mesonic rates as follows: $\Gamma_1 = \Gamma_n + \Gamma_p \equiv \Gamma(\Lambda n \rightarrow nn) + \Gamma(\Lambda p \rightarrow np)$ and $\Gamma_2 = \Gamma_{nn} + \Gamma_{np} + \Gamma_{pp} \equiv \Gamma(\Lambda nn \rightarrow nnn) + \Gamma(\Lambda np \rightarrow nnp) + \Gamma(\Lambda pp \rightarrow npp)$.

One should note that, strictly speaking, the only observables in hypernuclear weak decay are the lifetime τ , the mesonic rates Γ_{π^-} and Γ_{π^0} and the spectra of the emitted particles (nucleons, pions and photons). None of the above non-mesonic partial decay rates (Γ_n , Γ_p , Γ_{np} , etc) is an observable from a quantum-mechanical point of view. Each one of the possible elementary non-mesonic decays occurs in the nuclear environment, thus subsequent final

state interactions (FSI) modify the quantum numbers of the weak decay nucleons and new, secondary nucleons are emitted as well: this prevents the measurement of any of the non-mesonic partial decay rates. Instead, the total width Γ_T can be measured: being an inclusive quantity, for such a measurement one has to detect any of the possible products of either mesonic or non-mesonic decays (typically protons from non-mesonic decays). The fact that the detected particles undergo FSI does not appreciably alter the lifetime measurement, since strong interactions proceed on a much shorter time scale than weak decays, and $\tau^{\text{measured}} = \tau + \tau^{\text{strong}} \simeq \tau \equiv \hbar/\Gamma_T$.

In order to achieve a proper knowledge of the various decay mechanisms (in particular of the strangeness-changing baryon-baryon interactions), a meaningful comparison between theory and experiment must be possible. The above discussion shows that such a comparison requires the introduction of non-standard theoretical definitions for the non-mesonic partial decay rates (which, as mentioned, are not quantum-mechanical observables) together with the corresponding experimental methods for determining these rates. In our opinion, this point has not been adequately addressed in previous works and, among others, it has impacted on the well-known puzzle on the ratio Γ_n/Γ_p between the neutron- and the proton-induced non-mesonic rates.

In order to explain how the total non-mesonic rate can be determined in an experiment, we have to discuss first the measurement of the mesonic rates. The pion and nucleon emitted in a mesonic decay both have a momentum of about 100 MeV/c. Nucleons of a few MeV kinetic energy cannot be observed as they are below the experimental detection thresholds. Mesonic decays are thus identified by measuring pions (π^- 's or $\pi^0 \rightarrow \gamma\gamma$ decays). The mesonic width Γ_{π^-} (Γ_{π^0}) is determined from the observed π^- ($\pi^0 \rightarrow \gamma\gamma$) energy spectra and the total width Γ_T . For instance, $\Gamma_{\pi^-}^{\text{exp}} = (N_{\pi^-}/N_{\text{hyp}})\Gamma_T^{\text{exp}}$, N_{π^-} being the total number of detected π^- 's and N_{hyp} the total number of produced hypernuclei. Both these numbers are corrected for the detection efficiencies and the detector acceptances implied in the measurements. The mesonic rates measured in this way thus include the effect of in-medium pion renormalization. Theoretical models [7, 8] also taking into account distorted pion waves obtained mesonic widths in agreement with the experimental values (in particular, the importance of the pion wave-function distortion was first demonstrated in the works of Ref. [7]).

The experimental total non-mesonic rate is then obtained as the difference between the

total and the mesonic rates, $\Gamma_{\text{NM}}^{\text{exp}} = \Gamma_{\text{T}}^{\text{exp}} - \Gamma_{\text{M}}^{\text{exp}}$. The experimental determination of Γ_n/Γ_p is much more involved. Indeed, this ratio must be extracted from the nucleon emission spectra, and this requires some theoretical input [10, 11]. FSI are very important for the non-mesonic processes and nucleons which have or have not suffered FSI are indistinguishable between each other. A theoretical simulation of nucleon FSI is thus needed and, in principle, a coherent sum of both kinds of nucleons must be considered when evaluating the spectra. Generally, FSI are accounted for by an intranuclear cascade model [9], which is a semi-classical scheme.

In the present work we study the non-mesonic weak decay of hypernuclei ranging from ${}_{\Lambda}^{11}\text{B}$ to ${}_{\Lambda}^{208}\text{Pb}$ by using a nuclear matter approach implemented in a local density approximation. All the possible isospin channels for one- and two-body induced mechanisms are included in a microscopic approach based on the evaluation of Goldstone diagrams. The partial decay rates are derived by starting from a two-body weak transition potential. In particular, we investigate the effect of ground state correlations (GSC), i.e., the contribution of nucleon-nucleon correlations in the hypernucleus ground state. Leading order GSC contributions will be introduced on the same ground for one- and two-nucleon induced processes for the first time. The general formalism we adopt was established in Refs. [12, 13]. The weak transition potential for the nucleon-nucleon strong interaction contributing to the GSC we adopt a Bonn potential with the exchange of π , ρ , σ and ω mesons.

The paper is organized as follows. In Section II we start with general considerations about FSI, the definitions we employ for the weak decay rates as well as the method usually employed for the determination of Γ_n/Γ_p from data on nucleon spectra. In Section III we present and discuss the general framework for the evaluation of the one- and two-nucleon induced decay widths with the inclusion of GSC. In Section IV we make some further considerations about the evaluation of the widths and we discuss some former work on the subject. Explicit expressions for the considered GSC diagrams contributing to the one-nucleon induced rates are given in Section V and in Appendix A. Then, in Section VI we present our results and finally in Section VII some conclusions are given.

II. PRELIMINARY CONSIDERATIONS ON FSI EFFECTS AND ON THE DETERMINATION OF THE WEAK DECAY RATES

The Γ_n/Γ_p ratio is defined as the ratio between the total number of primary (i.e., weak decay) neutron–neutron and neutron–proton pairs, N_{nn}^{wd} and N_{np}^{wd} , emerging from the processes $\Lambda n \rightarrow nn$ and $\Lambda p \rightarrow np$, respectively. Due to nucleon final state interactions and two–body induced decays, the following inequality is expected for the observables nn and np coincidence numbers, N_{nn} and N_{np} [10] [35]:

$$\frac{\Gamma_n}{\Gamma_p} \equiv \frac{N_{nn}^{\text{wd}}}{N_{np}^{\text{wd}}} \neq \frac{N_{nn}}{N_{np}} . \quad (1)$$

Only N_{nn}/N_{np} is a quantum–mechanical observable: generally, its measurement is affected by thresholds on the nucleon energy and the pair opening angle [6, 14, 15]. Theoretical models are thus required to determine the “experimental” value of Γ_n/Γ_p from a measurement of N_{nn}/N_{np} . This unusual procedure to determine $(\Gamma_n/\Gamma_p)^{\text{exp}}$ makes complete sense provided different models are at disposal and lead to the same extracted ratio: only in such a case one is allowed to define this value as the experimental result for Γ_n/Γ_p . It is thus important to explore the predictions of alternative models when applied to the analysis of data. In the present section we go deeper into questions of this kind to show some ambiguities which need to be emphasized for a meaningful comparison between theory and experiment.

Let us first illustrate in some detail the procedure normally adopted to extract $(\Gamma_n/\Gamma_p)^{\text{exp}}$ from measurements of N_{nn}/N_{np} [10, 11]. Each one of the non–mesonic weak decay channel takes place by the emission of two or three primary nucleons. These nucleons propagate within the nuclear environment and cannot be measured. The strong interactions with the surrounding nucleons can change the charge and the energy–momentum of the primary nucleons; some of them can be absorbed by the medium and the emission of additional (secondary) nucleons can occur as well. All these processes are generically designated as final state interactions (FSI): they do not have to be included when calculating the decay rates, but the observable nucleon spectra, i.e., N_{nn} and N_{np} , are crucially affected by them. One has to emphasize that, on the contrary, baryon–baryon short range correlations in both the initial and the final states as well as mean field effects on the single particle wave–functions are genuine contributions to the decay rates.

FSI pertain to the same quantum–mechanical problem which starts with the Λ decay and

ends with the detection of the particles emitted by the hypernucleus. In a strict quantum-mechanical scheme, FSI cannot thus be disentangled from the weak interaction part of the problem: this is an analogous way of expressing the fact that the weak decay rates are not measurable. However, up to now FSI have been simulated by means of semi-classical models, i.e., by intranuclear cascade codes (INC) [9] acting after the weak decay, thus losing quantum-mechanical coherence. In such INC analyses, both one- and two-nucleon induced decays are included as inputs and one proceeds to fit N_{nn}/N_{np} data in order to determine the value of $(\Gamma_n/\Gamma_p)^{\text{exp}}$. Technically, this is achieved by applying Eq. (16) of Ref. [11] (see also Eqs. (1) and (2) of Ref. [10] and Eq. (3.14) of Ref. [16]), which is an exact relation only neglecting quantum coherence among the final, observable nucleons. Note that such a procedure also requires a theoretical estimate for the ratio Γ_2/Γ_1 . In other words, present nucleon-nucleon coincidence data only allows us to determine a correlation property between Γ_n/Γ_p and Γ_2/Γ_1 .

In general terms, one could wonder if it is possible to identify those quantum-mechanical contributions whose classical limit leads to a factorization between the weak decay process and the INC rescattering. This is a relevant question since in the theoretical evaluation of the non-mesonic decay rates FSI contributions must not be included; one indeed aims to extract the contribution of the elementary $\Lambda N \rightarrow nN$ and $\Lambda nn \rightarrow nNN$ processes by studying hypernuclear decay. Unfortunately, the above question does not seem to have a simple solution. Although we make here some considerations about this point, we believe that a complete answer to it goes beyond the present contribution.

Let us illustrate, by using an example, the nature of the problem. Consider the Λ self-energy diagram (a) of Fig. 1. This is a (time-ordered) Goldstone diagram where the weak transition potential $V^{\Lambda N \rightarrow NN}$, which is a two-body operator, produces an intermediate $2p1h$ configuration; afterwards, the action of the nucleon-nucleon strong interaction V^{NN} creates a further $1p1h$ pair and leads to a $3p2h$ final state. In terms of amplitudes, $V^{\Lambda N \rightarrow NN}$ produces two nucleons, one of which then strongly interacts with another nucleon, ending in the emission of three nucleons. Since the potential V^{NN} acts after $V^{\Lambda N \rightarrow NN}$, diagram (a) contains a FSI effect and we argue that it must not be included when evaluating the non-mesonic decay rate. Note that the idea of an interaction taking place after or before another one is a valid statement here as we are working with Goldstone diagrams. On the contrary, diagram (b) of Fig. 1 represents a ground state correlation (GSC) effect. It corresponds to

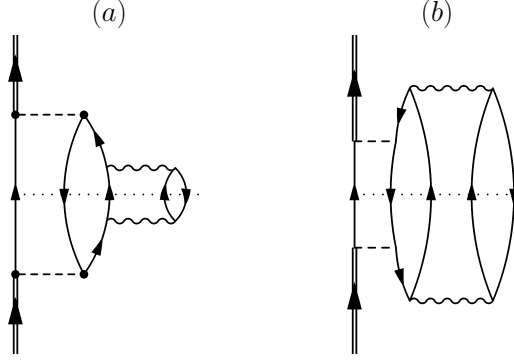


FIG. 1: Goldstone diagrams for FSI (a) and $2p2h$ GSC contributions (b) for three nucleon emission. The dashed and wavy lines stand for the potentials $V^{\Lambda N \rightarrow NN}$ and V^{NN} , respectively. The diagram (a) has poles on the $2p1h$ and $3p2h$ configurations, while (b) has a single pole on the $3p2h$ configuration. For the present discussion we only consider the $3p2h$ poles indicated by the dotted lines.

an amplitude in which the Λ decays by interacting with a correlated nucleon pair. Since the nucleon–nucleon interaction takes place before the action of the weak transition, this diagram must be considered when evaluating the decay rate Γ_2 .

Note also that the Goldstone diagrams (a) and (b) are two different time orderings of the same Feynman diagram. If Γ_2 were an observable, it would have to be evaluated by means of Feynman rather than Goldstone diagrams; both diagrams (a) and (b) would contribute to Γ_2 . These diagrams must actually be taken into account when evaluating the observable nucleon spectra. However, here we argue that, since Γ_2 is not an observable, some of the Goldstone diagram should not be included in the theoretical definition of this rate. The class of diagrams that does not contribute to Γ_2 depends on the definition one adopts for FSI. Our definition leaves aside those Goldstone diagrams, like diagram (a) in Fig. 1, in which at least one nucleon–nucleon interaction takes place after the weak transition potential. If on the other hand one were to include diagram (b) in the calculation of the widths, then it would not be clear how to identify the diagrams incorporating FSI effects.

A similar analysis to the previous one holds for the one–nucleon induced rates. Summarizing, we assume that one– and two–nucleon induced decay widths, which are not observables, are interpreted in terms of Goldstone diagrams in which no FSI effect is present. All the Goldstone diagrams in which at least one nucleon–nucleon interaction takes place after the weak transition potential must not be included when evaluating the decay rates. Any Gold-

stone diagram representing a GSC is instead a genuine contribution to the rates. In the calculation of the observable nucleon spectra, a description in terms of Feynman diagrams must instead be employed.

III. MANY-BODY TERMS IN THE NON-MESONIC DECAY RATES

Let us consider the one and two-body induced non-mesonic weak decay width for a Λ -hyperon with four-momentum $k = (k_0, \mathbf{k})$ inside infinite nuclear matter with Fermi momentum k_F . In a schematic way, one can write:

$$\Gamma_{1(2)}(k, k_F) = \sum_f |\langle f | V^{\Lambda N \rightarrow NN} | 0 \rangle_{k_F}|^2 \delta(E_f - E_0), \quad (2)$$

where $|0\rangle_{k_F}$ and $|f\rangle$ are the initial hypernuclear ground state (whose energy is E_0) and the possible $2p1h$ or $3p2h$ final states, respectively. The $2p1h$ ($3p2h$) final states define Γ_1 (Γ_2). The final state energy is E_f and $V^{\Lambda N \rightarrow NN}$ is the two-body weak transition potential.

The decay rates for a finite hypernucleus are obtained by the local density approximation [17], i.e., after averaging the above partial width over the Λ momentum distribution in the considered hypernucleus, $|\tilde{\psi}_\Lambda(\mathbf{k})|^2$, and over the local Fermi momentum, $k_F(r) = \{3\pi^2\rho(r)/2\}^{1/3}$, $\rho(r)$ being the density profile of the hypernuclear core. One thus has:

$$\Gamma_{1(2)} = \int d\mathbf{k} |\tilde{\psi}_\Lambda(\mathbf{k})|^2 \int d\mathbf{r} |\psi_\Lambda(\mathbf{r})|^2 \Gamma_{1(2)}(\mathbf{k}, k_F(r)), \quad (3)$$

where for $\psi_\Lambda(\mathbf{r})$, the Fourier transform of $\tilde{\psi}_\Lambda(\mathbf{k})$, we adopt the $1s_{1/2}$ harmonic oscillator wave-function with frequency $\hbar\omega$ ($= 10.8$ MeV for ^{12}C) adjusted to the experimental energy separation between the s and p Λ -levels in the considered hypernucleus. The Λ total energy in Eqs. (2) and (3) is given by $k_0 = m_\Lambda + \mathbf{k}^2/(2m_\Lambda) + V_\Lambda$, V_Λ ($= -10.8$ MeV for ^{12}C) being a binding energy term.

Since $V^{\Lambda N \rightarrow NN}$ is a two-body operator, the emission of two nucleons is originated either from the Hartree-Fock vacuum or from GSC induced by the nucleon-nucleon interaction. At variance, the emission of three nucleons can be only achieved when $V^{\Lambda N \rightarrow NN}$ acts over a GSC. It is therefore convenient to introduce the following hypernuclear ground state wave-function [18]:

$$|0\rangle_{k_F} = \mathcal{N}(k_F) \left(| \rangle - \sum_{p,h,p',h'} \frac{\langle php'h' | V^{NN} | \rangle_{D+E}}{\varepsilon_p - \varepsilon_h + \varepsilon_{p'} - \varepsilon_{h'}} | php'h' \rangle \right) \otimes | p_\Lambda \rangle, \quad (4)$$

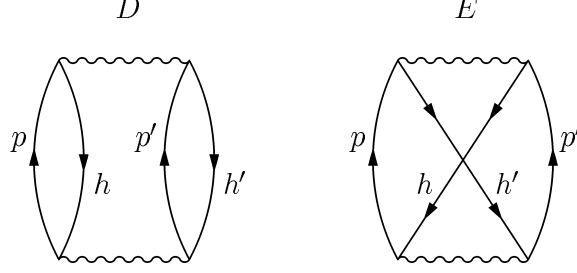


FIG. 2: Direct (D) and exchange (E) Goldstone diagrams for the $2p2h$ GSC induced by the nuclear residual interaction V^{NN} .

where $|\rangle$ is the uncorrelated core ground state wave-function, i.e., the Hartree-Fock vacuum, while the second term in the rhs represents $2p2h$ correlations and contains both direct (D) and exchange (E) matrix elements of the nuclear residual interaction V^{NN} . Besides, $|p_\Lambda\rangle$ is the normalized state of the Λ , the particle and hole energies are denoted by ε_i and:

$$\mathcal{N}(k_F) = \left(1 + \sum_{p,h,p',h'} \left| \frac{\langle php'h' | V^{NN} | \rangle_{D+E}}{\varepsilon_p - \varepsilon_h + \varepsilon_{p'} - \varepsilon_{h'}} \right|^2 \right)^{-1/2} \quad (5)$$

is the ground state normalization function. The particular labeling of Eqs. (4) and (5) is explained in Fig. 2. The explicit expression for $\mathcal{N}(k_F)$ is given in Ref. [19].

By inserting Eq. (4) into Eq. (2), for Γ_1 one obtains:

$$\begin{aligned} \Gamma_1(\mathbf{k}, k_F) &= \mathcal{N}^2(k_F) \sum_f \delta(E_f - E_0) \left| \langle f | V^{\Lambda N \rightarrow NN} | p_\Lambda \rangle_{D+E} \right. \\ &\quad \left. - \sum_{p,h,p',h'} \langle f | V^{\Lambda N \rightarrow NN} | php'h' \rangle_{D+E} \frac{\langle php'h' ; p_\Lambda | V^{NN} | p_\Lambda \rangle_{D+E}}{\varepsilon_p - \varepsilon_h + \varepsilon_{p'} - \varepsilon_{h'}} \right|^2, \end{aligned} \quad (6)$$

the final states $|f\rangle$ being restricted to $2p1h$ states. For Γ_2 one has:

$$\begin{aligned} \Gamma_2(\mathbf{k}, k_F) &= \mathcal{N}^2(k_F) \sum_f \delta(E_f - E_0) \\ &\quad \times \left| \sum_{p,h,p',h'} \langle f | V^{\Lambda N \rightarrow NN} | php'h' \rangle_{D+E} \frac{\langle php'h' ; p_\Lambda | V^{NN} | p_\Lambda \rangle_{D+E}}{\varepsilon_p - \varepsilon_h + \varepsilon_{p'} - \varepsilon_{h'}} \right|^2, \end{aligned} \quad (7)$$

where the final states are given by $3p2h$ states. Note that all the matrix elements of V^{NN} and $V^{\Lambda N \rightarrow NN}$ appear in the antisymmetrized form.

Let us focus now on the kind of diagrams contributing to Γ_1 and Γ_2 . This discussion is done in terms of transition amplitudes rather than self-energies. In Fig. 3 we report

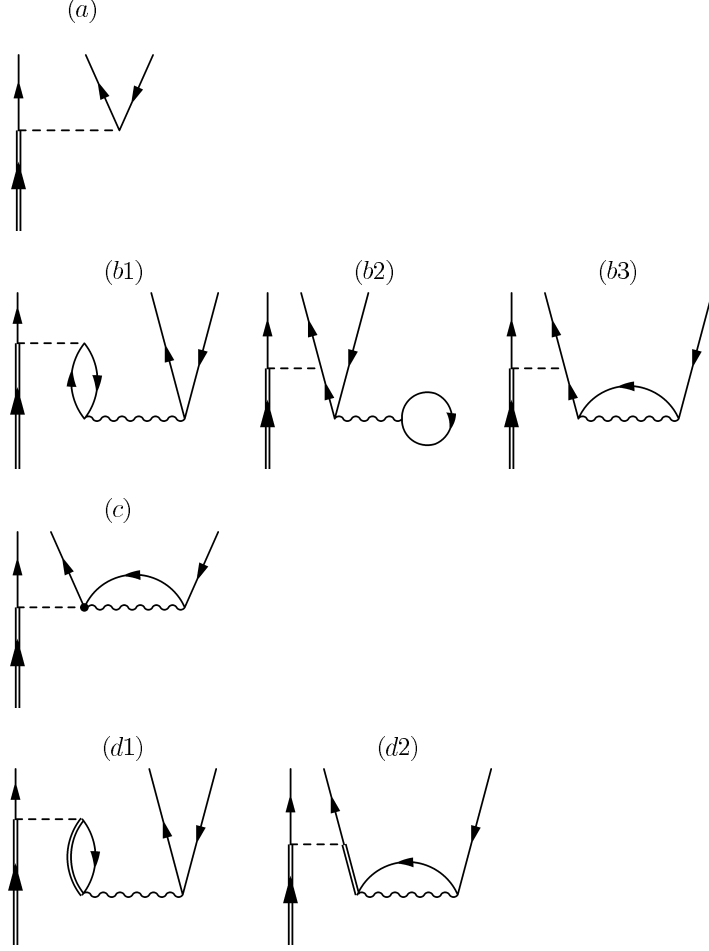


FIG. 3: Transition amplitudes contributing to Γ_1 . A double-line (without arrow) represents the $\Delta(1232)$ resonance.

some of the most representative transition amplitudes which contribute to Γ_1 . All diagrams but (a) are originated by a GSC. Only the contribution of diagram (a) to Γ_1 has been calculated microscopically up to now. The line (b) represents typical $2p2h$ correlations. The contribution (c) is a contact term involving a $\pi\pi NN$ strong vertex, while line (d) represents the contribution of the $\Delta(1232)$ resonance. It should be mentioned that there has been a great deal of controversy around the theoretical determination of the Γ_n/Γ_p ratio and the challenging comparison with data. In these discussions, all theoretical efforts have been devoted to the (a) term only; the remaining ones have simply been ignored.

A similar analysis can be done for Γ_2 starting from the amplitudes of Fig. 4. Again, only the (a) term has been evaluated up to now in microscopic calculations [13]. The graphs in Figs. 3 and 4 are only representative cases. For instance, also the amplitude of Fig. 5

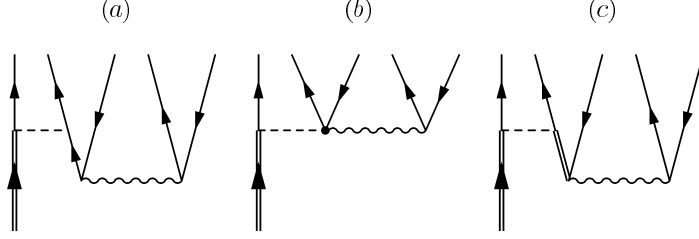


FIG. 4: Transition amplitudes contributing to Γ_2 .

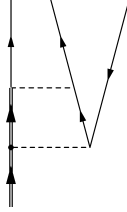


FIG. 5: Transition amplitude contributing to Γ_1 and involving a strong interaction $V^{\Lambda N}$ between the hyperon and a $1p1h$ pair.

should be included when calculating Γ_1 . Unlike the other amplitudes of Figures. 3 and 4, the one in Fig. 5 involves a strong interaction $V^{\Lambda N}$ between the Λ and a $1p1h$ pair (i.e., a $1p1h$ GSC) and then the usual action of the weak transition potential. Apart from the explicit calculation, such a contribution could in principle be included in an effective way through the calculation of diagram (a) of Fig. 3 with a suitably chosen weak transition potential $V^{\Lambda N \rightarrow NN}$. However, based on the absence of isovector-meson exchange in the strong potential $V^{\Lambda N}$, one may anticipate a small effect of this amplitude. Other amplitudes will provide important contributions. In the graph (a) of Fig. 4 the weak transition potential can also be connected to a hole line [13]. In addition, since V^{NN} and $V^{\Lambda N \rightarrow NN}$ are two-body operators whose matrix elements are antisymmetrized, Pauli exchange terms must be considered as well [19].

All the graphs in Figs. 3 and 4 have the same initial state, which is the hypernuclear ground state. The final state of the graphs in Fig. 3 (Fig. 4) is a $2p1h$ ($3p2h$) state. To obtain the various decay width, all graphs representing transitions amplitudes with the same initial and final states are added and then squared. For instance, from Fig. 4 one obtains a total of six direct diagrams: the square of each individual amplitude plus the three interference terms. For the amplitudes in Fig. 3 there is a total of twenty-eight different direct terms. In addition, antisymmetrization considerably increases the amount of diagrams. From our

previous works it is clear to us that a full microscopic evaluation of each term is mandatory for several reasons. First, a raw estimation of a remarkable amount of different diagrams makes the final result quite uncertain. Secondly, there is no ground to evaluate differently the diagrams originated from Fig. 3 and those from Fig. 4: once a microscopic calculation is performed for the square of diagrams (*a*) of Figs. 3 and 4, the same should be done for the remaining contributions, which are all leading order GSC contributions.

In the present work, as a further step towards the calculation of the whole set of diagrams relevant for the non-mesonic decay, the one-nucleon induced widths originated from the sum of the transition amplitudes (*a*) plus (*b1*) of Fig. 3 are evaluated for the first time. Accordingly, the two-nucleon induced rates are instead obtained from the amplitude (*a*) of Fig. 4 by following Ref. [19]. Antisymmetrization is coherently applied to all contributions. Before proceeding with the formal derivation of the decay widths, in the next Section we first point out additional observations on the evaluation of the decay rates and on previous, related work.

IV. FURTHER CONSIDERATIONS ON THE EVALUATION OF THE WEAK DECAY RATES

Let us start this discussion by paying attention to the twofold effect of the nuclear residual interaction V^{NN} within the matrix elements of Eq. (2). When V^{NN} acts on the uncorrelated hypernuclear ground state $|i\rangle$, as in Eq. (4), one has a GSC. Alternatively, V^{NN} may introduce medium effects on the weak transition potential $V^{\Lambda N \rightarrow NN}$. Both effects must be taken into account when calculating the decay rates. In addition, V^{NN} may modify the final states $|f\rangle = |2p1h\rangle$ or $|3p2h\rangle$: for instance, acting on a $|2p1h\rangle$ final state, it can produce a $|3p2h\rangle$ state, as in Fig. 1(a); this results in a FSI which does not contribute to Eq. (2).

Concerning the medium effects previously mentioned, let us discuss some aspects of the work of Ref. [20]. Here, V^{NN} introduces medium modifications on the mesons propagators appearing in $V^{\Lambda N \rightarrow NN}$ through the direct part of the RPA (ring approximation): schematically, in our scheme one simply has to replace $V^{\Lambda N \rightarrow NN}$ with $\tilde{V}^{\Lambda N \rightarrow NN} = V^{\Lambda N \rightarrow NN} / |1 - \Pi V^{NN}|$, where the polarization propagator Π contains $1p1h$ and $1\Delta 1h$ contributions in Ref. [20]. Note that, since only the absolute value of the ring propagator is kept, the modified weak transition potential remains a real function. This approach thus

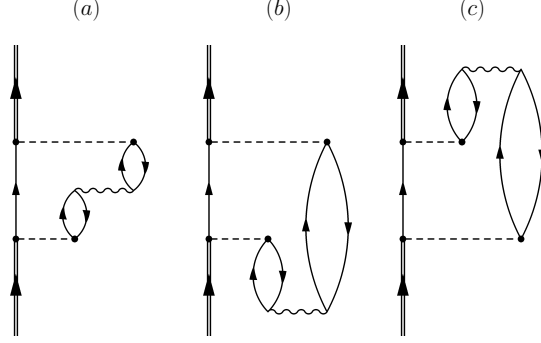


FIG. 6: Goldstone diagrams for FSI (a) and $2p2h$ GSC contributions (b) and (c) leading to two nucleon emission.

represents a refinement of the weak transition potential and is consistent with Eq. (2).

We emphasize that the mere use of diagrams when discussing the formalism developed in Ref. [20] or the present one could be misleading. For the approximation considered in Ref. [20], in Eq. (2) one has to employ the matrix element $\langle f | \tilde{V}^{\Lambda N \rightarrow NN} | 0 \rangle_{D+E}$ of the modified weak transition potential (the corresponding direct and exchange self-energy diagrams are shown in Fig. 2 in Ref. [20]). By making an expansion of the square of this matrix element in the ring series, the two terms at first order in V^{NN} correspond to a self-energy contribution which matches exactly with the (a) diagram in Fig. 6, where the final state $|f\rangle = |2p1h\rangle$ corresponds either to the upper or the lower bubble. Nevertheless, the same diagram could also be associated to the direct part of the following product of matrix elements: $\langle f | V^{NN} | i \rangle_{D+E} \langle i | V^{\Lambda N \rightarrow NN} | 0 \rangle_{D+E}$, where $|i\rangle$ is a $2p1h$ intermediate configuration. But, since this product contains a FSI, it is not a correct contribution to the decay rates of Eq. (2). Antisymmetry of this product of matrix elements gives rise to a total of eight self-energy diagrams, which are shown in Fig. 4 in Ref. [21] and used there to calculate the (observable) spectra of the non-mesonic weak decay nucleons. From the analytical point of view, the product $\langle f | V^{NN} | i \rangle_{D+E} \langle i | V^{\Lambda N \rightarrow NN} | 0 \rangle_{D+E}$ is clearly different from the term at first order in V^{NN} entering $\langle f | \tilde{V}^{\Lambda N \rightarrow NN} | 0 \rangle_{D+E}$. When the comparison is done using the full set of direct plus exchange diagrams, FSI and the medium modifications on the weak transition potential are manifestly different effects. Only the latter can be included in the calculation of the decay rates.

As a final remark for this section, we observe that the amplitudes (a) and (b1) of Fig. 3 produce the self-energy diagrams (b) and (c) of Fig. 6. They are GSC terms and thus

contribute to the decay rates. Conversely, the (a) diagram of Fig. 6 must be left aside in the calculation, unless one considers it as a medium modification on the weak transition potential (but then, other medium modification contributions should be considered simultaneously), as done in Ref. [20]. The Goldstone diagrams of Fig. 6 are the three possible time orderings of the same Feynman diagram. Again, we stress that the fact that one out of three diagrams in Fig. 6 will not be included in our calculation of the decay rates makes sense since these rates are not observables and thus do not have to be described by Feynman diagrams.

V. FORMAL DERIVATION OF THE DECAY RATES Γ_n AND Γ_p INCLUDING GSC

In Fig. 3 we have shown a set of amplitudes which contribute to the decay rate Γ_1 of Eq. (2). Only the amplitude (a) has been evaluated explicitly up to now. In the present work we extend the microscopic approach to include the amplitude (b1), which originates from GSC contributions that we expect to be important.

Before proceeding with the derivation of decay widths, it is convenient to give the expressions for the potentials. The weak transition potential $V^{\Lambda N \rightarrow NN}$ and the nuclear residual interaction V^{NN} read:

$$V^{\Lambda N \rightarrow NN(NN)}(q) = \sum_{\tau_{\Lambda(N)}=0,1} \mathcal{O}_{\tau_{\Lambda(N)}} \mathcal{V}_{\tau_{\Lambda(N)}}^{\Lambda N \rightarrow NN(NN)}(q) , \quad (8)$$

where the isospin dependence is given by

$$\mathcal{O}_{\tau_{\Lambda(N)}} = \begin{cases} 1 & \text{for } \tau_{\Lambda(N)} = 0 \\ \boldsymbol{\tau}_1 \cdot \boldsymbol{\tau}_2 & \text{for } \tau_{\Lambda(N)} = 1 . \end{cases} \quad (9)$$

The values 0 and 1 for $\tau_{\Lambda(N)}$ refer to the isoscalar and isovector parts of the interactions, respectively. The spin and momentum dependence of the weak transition potential is given by:

$$\begin{aligned} \mathcal{V}_{\tau_{\Lambda}}^{\Lambda N \rightarrow NN}(q) = & (G_F m_\pi^2) \{ S_{\tau_{\Lambda}}(q) \boldsymbol{\sigma}_1 \cdot \hat{\mathbf{q}} + S'_{\tau_{\Lambda}}(q) \boldsymbol{\sigma}_2 \cdot \hat{\mathbf{q}} + P_{C,\tau_{\Lambda}}(q) \\ & + P_{L,\tau_{\Lambda}}(q) \boldsymbol{\sigma}_1 \cdot \hat{\mathbf{q}} \boldsymbol{\sigma}_2 \cdot \hat{\mathbf{q}} + P_{T,\tau_{\Lambda}}(q) (\boldsymbol{\sigma}_1 \times \hat{\mathbf{q}}) \cdot (\boldsymbol{\sigma}_2 \times \hat{\mathbf{q}}) \\ & + i S_{V,\tau_{\Lambda}}(q) (\boldsymbol{\sigma}_1 \times \boldsymbol{\sigma}_2) \cdot \hat{\mathbf{q}} \} , \end{aligned} \quad (10)$$

where the functions $S_{\tau_{\Lambda}}(q)$, $S'_{\tau_{\Lambda}}(q)$, $P_{C,\tau_{\Lambda}}(q)$, $P_{L,\tau_{\Lambda}}(q)$, $P_{T,\tau_{\Lambda}}(q)$ and $S_{V,\tau_{\Lambda}}(q)$, which include short range correlations, are adjusted to reproduce any weak transition potential.

The corresponding expression for the nuclear residual interaction is given by:

$$\begin{aligned} \mathcal{V}_{\tau_N}^{NN}(q) = & \frac{f_\pi^2}{m_\pi^2} \{ \mathcal{V}_{C,\tau_N}(q) + \mathcal{V}_{L,\tau_N}(q) \boldsymbol{\sigma}_1 \cdot \hat{\mathbf{q}} \boldsymbol{\sigma}_2 \cdot \hat{\mathbf{q}} \\ & + \mathcal{V}_{T,\tau_N}(q) (\boldsymbol{\sigma}_1 \times \hat{\mathbf{q}}) \cdot (\boldsymbol{\sigma}_2 \times \hat{\mathbf{q}}) \} , \end{aligned} \quad (11)$$

where the functions $\mathcal{V}_{C,\tau_N}(q)$, $\mathcal{V}_{L,\tau_N}(q)$ and $\mathcal{V}_{T,\tau_N}(q)$ are also adjusted to reproduce any nuclear residual interaction.

In particular, $V^{\Lambda N \rightarrow NN}$ is represented by the exchange of the π , η , K , ρ , ω and K^* mesons, within the formulation of Ref. [22], with strong coupling constants and cut-off parameters deduced from the Nijmegen soft-core interaction NSC97f of Ref. [23]. For V^{NN} we have used a Bonn potential [24] in the framework of the parametrization presented in Ref. [25], which contains the exchange of π , ρ , σ and ω mesons.

We give now explicit expressions for the partial decay width $\Gamma_1(\mathbf{k}, k_F)$ of Eq. (6), which for convenience is expressed in terms of its isospin components $\Gamma_n(\mathbf{k}, k_F)$ and $\Gamma_p(\mathbf{k}, k_F)$. Let us first rewrite Eq. (6) as follows:

$$\Gamma_{n(p)}(\mathbf{k}, k_F) = \Gamma_{n(p)}^0(\mathbf{k}, k_F) + \Gamma_{n(p)}^{0-\text{GSC}}(\mathbf{k}, k_F) + \Gamma_{n(p)}^{\text{GSC}}(\mathbf{k}, k_F) , \quad (12)$$

where:

$$\begin{aligned} \Gamma_{n(p)}^0(\mathbf{k}, k_F) &= \mathcal{N}^2(k_F) \sum_f \delta(E_f - E_0) \left| \langle f | V^{\Lambda N \rightarrow NN} | p_\Lambda \rangle_{D+E} \right|^2 , \\ \Gamma_{n(p)}^{0-\text{GSC}}(\mathbf{k}, k_F) &= -2\mathcal{N}^2(k_F) \sum_f \sum_{p,h,p',h'} \delta(E_f - E_0) \langle p_\Lambda | (V^{\Lambda N \rightarrow NN})^\dagger | f \rangle_{D+E} \\ &\quad \times \langle f | V^{\Lambda N \rightarrow NN} | p h p' h' ; p_\Lambda \rangle_{D+E} \frac{\langle p h p' h' ; p_\Lambda | V^{NN} | p_\Lambda \rangle_{D+E}}{\varepsilon_p - \varepsilon_h + \varepsilon_{p'} - \varepsilon_{h'}} , \\ \Gamma_{n(p)}^{\text{GSC}}(\mathbf{k}, k_F) &= \mathcal{N}^2(k_F) \sum_f \sum_{p,h,p',h'} \delta(E_f - E_0) \left| \langle f | V^{\Lambda N \rightarrow NN} | p h p' h' ; p_\Lambda \rangle_{D+E} \right. \\ &\quad \left. \times \frac{\langle p h p' h' ; p_\Lambda | V^{NN} | p_\Lambda \rangle_{D+E}}{\varepsilon_p - \varepsilon_h + \varepsilon_{p'} - \varepsilon_{h'}} \right|^2 . \end{aligned} \quad (13)$$

The first component, $\Gamma_{n(p)}^0$, is the contribution from the uncorrelated hypernuclear ground state, the third one, $\Gamma_{n(p)}^{\text{GSC}}$, result from ground state correlations, while $\Gamma_{n(p)}^{0-\text{GSC}}$ is the interference term between correlated and uncorrelated ground states.

It is now convenient to consider the following decomposition, dictated by the isospin

quantum number:

$$\begin{aligned}
\Gamma_{n(p)}^0(\mathbf{k}, k_F) &= \sum_{P,Q=D,E} \Gamma_{n(p)}^{PQ}(\mathbf{k}, k_F) \\
&= \sum_{P,Q=D,E} \sum_{\tau_{\Lambda'}, \tau_{\Lambda}=0,1} \mathcal{T}_{\tau_{\Lambda'}, \tau_{\Lambda}, n(p)}^{PQ} \Gamma_{\tau_{\Lambda'}, \tau_{\Lambda}}^{PQ}(\mathbf{k}, k_F), \\
\Gamma_{n(p)}^{0-\text{GSC}}(\mathbf{k}, k_F) &= \sum_{P,Q,Q'=D,E} \Gamma_{n(p)}^{PQQ'}(\mathbf{k}, k_F) \\
&= \sum_{P,Q,Q'=D,E} \sum_{\tau_{\Lambda'}, \tau_{\Lambda}, \tau_N=0,1} \mathcal{T}_{\tau_{\Lambda'}, \tau_{\Lambda}, \tau_N, n(p)}^{PQQ'} \Gamma_{\tau_{\Lambda'}, \tau_{\Lambda}, \tau_N}^{PQQ'}(\mathbf{k}, k_F), \\
\Gamma_{n(p)}^{\text{GSC}}(\mathbf{k}, k_F) &= \sum_{P',P,Q,Q'=D,E} \Gamma_{n(p)}^{P'PQQ'}(\mathbf{k}, k_F) \\
&= \sum_{P',P,Q,Q'=D,E} \sum_{\tau_{N'}, \tau_{\Lambda'}, \tau_{\Lambda}, \tau_N=0,1} \mathcal{T}_{\tau_{N'}, \tau_{\Lambda'}, \tau_{\Lambda}, \tau_N, n(p)}^{P'PQQ'} \Gamma_{\tau_{N'}, \tau_{\Lambda'}, \tau_{\Lambda}, \tau_N}^{P'PQQ'}(\mathbf{k}, k_F),
\end{aligned} \tag{14}$$

where $P', P, Q, Q' = D$ or E refer to the direct or exchange character of the matrix elements of Eq. (13). The isospin factors are given by:

$$\begin{aligned}
\mathcal{T}_{\tau_{\Lambda'}, \tau_{\Lambda}, n(p)}^{PQ} &= \sum_{f, \text{isospin}} \langle t_{\Lambda} | \mathcal{O}_{\tau_{\Lambda'}} | f \rangle_P \langle f | \mathcal{O}_{\tau_{\Lambda}} | t_{\Lambda} \rangle_Q, \\
\mathcal{T}_{\tau_{\Lambda'}, \tau_{\Lambda}, \tau_N, n(p)}^{PQQ'} &= \sum_{f, \text{isospin}} \langle t_{\Lambda} | \mathcal{O}_{\tau_{\Lambda'}} | f \rangle_P \langle f | \mathcal{O}_{\tau_{\Lambda}} | t_p t_h t_{p'} t_{h'}, t_{\Lambda} \rangle_Q \\
&\quad \times \langle t_p t_h t_{p'} t_{h'}, t_{\Lambda} | \mathcal{O}_{\tau_N} | t_{\Lambda} \rangle_{Q'}, \\
\mathcal{T}_{\tau_{N'}, \tau_{\Lambda'}, \tau_{\Lambda}, \tau_N, n(p)}^{P'PQQ'} &= \sum_{f, \text{isospin}} \langle t_{\Lambda} | \mathcal{O}_{\tau_{N'}} | t_{\tilde{p}} t_{\tilde{h}} t_{\tilde{p}'} t_{\tilde{h}'}, t_{\Lambda} \rangle_{P'} \langle t_{\tilde{p}} t_{\tilde{h}} t_{\tilde{p}'} t_{\tilde{h}'}, t_{\Lambda} | \mathcal{O}_{\tau_{\Lambda'}} | f \rangle_P \\
&\quad \times \langle f | \mathcal{O}_{\tau_{\Lambda}} | t_p t_h t_{p'} t_{h'}, t_{\Lambda} \rangle_Q \langle t_p t_h t_{p'} t_{h'}, t_{\Lambda} | \mathcal{O}_{\tau_N} | t_{\Lambda} \rangle_{Q'},
\end{aligned}$$

where the summations run over all the isospin projections t 's, with the constrain that the

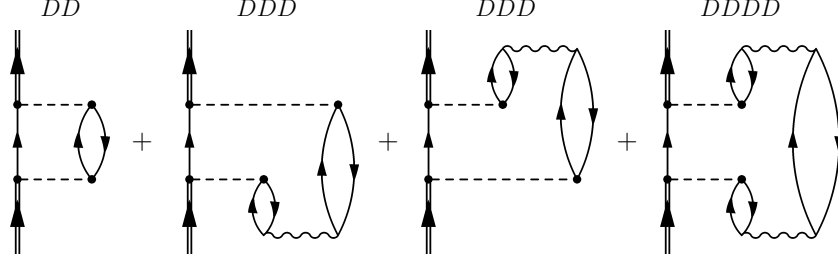


FIG. 7: Direct Goldstone diagrams corresponding to the square of the amplitude sum (a) + (b1) of Fig. 3. See the decomposition of Eq. (14).

emitted particles are nn for Γ_n and np for Γ_p . For the partial decay widths we instead find:

$$\Gamma_{\tau_{\Lambda'}\tau_{\Lambda}}^{PQ}(\mathbf{k}, k_F) = \mathcal{N}^2(k_F) (-1)^n \sum_f \delta(E_f - E_0) \quad (15)$$

$$\times \langle p_{\Lambda} | (\mathcal{V}_{\tau_{\Lambda'}}^{\Lambda N \rightarrow NN}(q'))^{\dagger} | f \rangle_P \langle f | \mathcal{V}_{\tau_{\Lambda}}^{\Lambda N \rightarrow NN}(q) | p_{\Lambda} \rangle_Q ,$$

$$\Gamma_{\tau_{\Lambda'}\tau_{\Lambda}\tau_N}^{PQQ'}(\mathbf{k}, k_F) = -2\mathcal{N}^2(k_F) (-1)^n \sum_f \sum_{p,h,p',h'} \delta(E_f - E_0) \quad (16)$$

$$\times \langle p_{\Lambda} | (\mathcal{V}_{\tau_{\Lambda'}}^{\Lambda N \rightarrow NN}(q'))^{\dagger} | f \rangle_P \langle f | \mathcal{V}_{\tau_{\Lambda}}^{\Lambda N \rightarrow NN}(q) | php'h'; p_{\Lambda} \rangle_Q$$

$$\times \frac{\langle php'h'; p_{\Lambda} | \mathcal{V}_{\tau_N}^{NN}(t) | p_{\Lambda} \rangle_{Q'}}{\varepsilon_p - \varepsilon_h + \varepsilon_{p'} - \varepsilon_{h'}} ,$$

$$\Gamma_{\tau_{\Lambda'}\tau_{\Lambda}\tau_{\Lambda}\tau_N}^{P'PQQ'}(\mathbf{k}, k_F) = \mathcal{N}^2(k_F) (-1)^n \sum_f \sum_{\tilde{p}, \tilde{h}, \tilde{p}', \tilde{h}'} \sum_{p,h,p',h'} \delta(E_f - E_0) \quad (17)$$

$$\times \frac{\langle p_{\Lambda} | (\mathcal{V}_{\tau_{\Lambda'}}^{NN}(t'))^{\dagger} | \tilde{p}, \tilde{h}, \tilde{p}', \tilde{h}' \rangle_{P'}}{\varepsilon_{\tilde{p}} - \varepsilon_{\tilde{h}} + \varepsilon_{\tilde{p}'} - \varepsilon_{\tilde{h}'}}$$

$$\times \langle \tilde{p}, \tilde{h}, \tilde{p}', \tilde{h}' \rangle_{P'} | (\mathcal{V}_{\tau_{\Lambda'}}^{\Lambda N \rightarrow NN}(q'))^{\dagger} | f \rangle_P$$

$$\times \langle f | \mathcal{V}_{\tau_{\Lambda}}^{\Lambda N \rightarrow NN}(q) | php'h'; p_{\Lambda} \rangle_Q$$

$$\times \frac{\langle php'h'; p_{\Lambda} | \mathcal{V}_{\tau_N}^{NN}(t) | p_{\Lambda} \rangle_{Q'}}{\varepsilon_p - \varepsilon_h + \varepsilon_{p'} - \varepsilon_{h'}} .$$

Note that the values of the energy–momentum carried by the particles and holes lines depends on the topology of the corresponding diagram, while n is the number of crossing between fermionic lines.

Let us now apply the above formalism to a model including the amplitudes (a) and (b1) of Fig. 3. Four direct self–energy diagrams correspond to the square of the amplitude sum (a) + (b1); they are given in Fig. 7. Note that these diagrams admits a single cut, giving rise to a $2p1h$ final state. The DD diagram contributes to the partial widths $\Gamma_{n(p)}^0$ of Eq. (14). The two DDD diagrams, which have the same numerical value and are interferences between

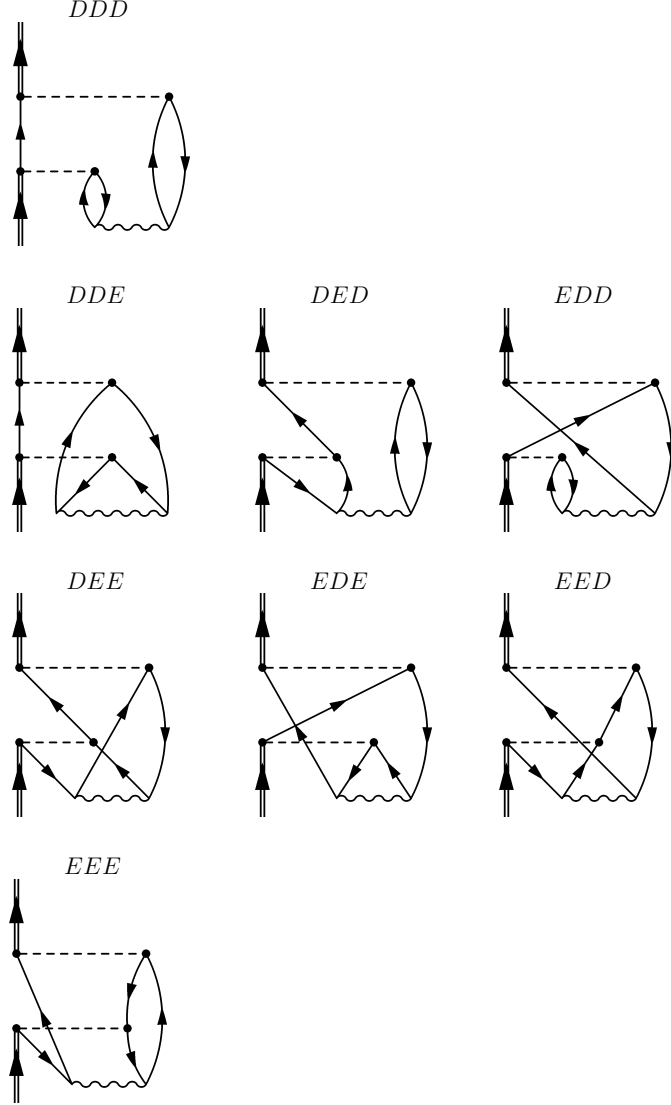


FIG. 8: Goldstone diagrams for the partial rates $\Gamma_{n(p)}^{PQQ'}$ contributing to Eq. (14).

the amplitudes (a) and (b1) of Fig. 3, are included in the partial widths $\Gamma_{n(p)}^{0-\text{GSC}}$. Finally, the diagram $DDDD$ contributes to $\Gamma_{n(p)}^{\text{GSC}}$. Many exchange diagrams are obtained from the antisymmetrized amplitude sum (a) + (b1): one PQ exchange diagram is the partner of the DD one of Fig. 7; seven PQQ' exchange diagrams are companions of each one of the DDD ones; fifteen $P'PQQ'$ exchange diagrams add to the $DDDD$ one.

Formal expressions for $\Gamma_{n(p)}^0$ can be found in Ref. [12]. The $\Gamma_{n(p)}^{PQQ'}$'s contributing to $\Gamma_{n(p)}^{0-\text{GSC}}$ (see Eq. (14)) correspond to the diagrams of Fig. 8. By replacing, in Eq. (16), the sum over momenta by integrals and by performing the energy integrations and the spin summation,

the following expression for $\Gamma_{\tau_{\Lambda'}\tau_{\Lambda}\tau_N}^{PQQ'}$ can be obtained:

$$\begin{aligned} \Gamma_{\tau_{\Lambda'}\tau_{\Lambda}\tau_N}^{PQQ'}(\mathbf{k}, k_F) &= \mathcal{N}^2(k_F) \frac{1}{4} \frac{(-1)^n}{(2\pi)^8} (G_F m_\pi^2)^2 \frac{f_\pi^2}{m_\pi^2} \\ &\times \int \int \int d\mathbf{q} d\mathbf{h} d\mathbf{h}' \mathcal{W}_{\tau_{\Lambda'}\tau_{\Lambda}\tau_N}^{PQQ'}(q, q', t) \\ &\times \Theta(k, q, q', t, h, h', k_F) \frac{1}{-\varepsilon_{2p2h}^{PQQ'}} \delta(q_0 - (\varepsilon_{\mathbf{h}'+\mathbf{q}} - \varepsilon_{\mathbf{h}})) , \end{aligned} \quad (18)$$

where $q_0 = k_0 - \varepsilon_{\mathbf{k}-\mathbf{q}} - V_N$, V_N being the nucleon binding energy, while the functions $\mathcal{W}_{\tau_{\Lambda'}\tau_{\Lambda}\tau_N}^{PQQ'}(q, q', t)$ and $\Theta(k, q, q', t, h, h', k_F)$ and the energy denominator $\varepsilon_{2p2h}^{PQQ'}$ are specific of each PQQ' contribution. The function $\mathcal{W}_{\tau_{\Lambda'}\tau_{\Lambda}\tau_N}^{PQQ'}(q, q', t)$ contains the momentum dependence of the nuclear residual interaction and the weak transition potentials and the spin summation, while $\Theta(k, q, q', t, h, h', k_F)$ is a product of step functions which defines the phase space of particles and holes.

In the present section we present the explicit expression for the direct term $\Gamma_{\tau_{\Lambda'}\tau_{\Lambda}\tau_N}^{DDD}$; the other seven ones are displayed in Appendix A. We obtain:

$$\begin{aligned} \Gamma_{\tau_{\Lambda'}\tau_{\Lambda}\tau_N}^{DDD}(\mathbf{k}, k_F) &= \mathcal{N}^2(k_F) \frac{1}{4} \frac{1}{(2\pi)^8} (G_F m_\pi^2)^2 \frac{f_\pi^2}{m_\pi^2} \\ &\times \int \int \int d\mathbf{q} d\mathbf{h} d\mathbf{h}' \mathcal{W}_{\tau_{\Lambda'}\tau_{\Lambda}\tau_N}^{DDD}(q) \\ &\times \theta(q_0) \theta(|\mathbf{k}-\mathbf{q}| - k_F) \theta(|\mathbf{q}-\mathbf{h}| - k_F) \theta(k_F - |\mathbf{h}|) \\ &\times \theta(|\mathbf{q}+\mathbf{h}'| - k_F) \theta(k_F - |\mathbf{h}'|) \\ &\times \frac{1}{-q_0 - (\varepsilon_{\mathbf{h}-\mathbf{q}} - \varepsilon_{\mathbf{h}})} \delta(q_0 - (\varepsilon_{\mathbf{h}'+\mathbf{q}} - \varepsilon_{\mathbf{h}})) . \end{aligned} \quad (19)$$

The expressions for $\Theta(k, q, q', t, h, h', k_F)$ and ε_{2p2h}^{DDD} are self-evident. Moreover:

$$\mathcal{W}_{\tau_{\Lambda'}\tau_{\Lambda}\tau_N}^{DDD}(q) = 8 \{ [S'_{\tau_{\Lambda'}}(q) S'_{\tau_{\Lambda}}(q) + P_{C,\tau_{\Lambda'}}(q) P_{C,\tau_{\Lambda}}(q)] \mathcal{V}_{C,\tau_N}(q) \quad (20)$$

$$\begin{aligned} &+ [S_{\tau_{\Lambda'}}(q) S_{\tau_{\Lambda}}(q) + P_{L,\tau_{\Lambda'}}(q) P_{L,\tau_{\Lambda}}(q)] \mathcal{V}_{L,\tau_N}(q) \\ &+ 2 [S_{V,\tau_{\Lambda'}}(q) S_{V,\tau_{\Lambda}}(q) + P_{T,\tau_{\Lambda'}}(q) P_{T,\tau_{\Lambda}}(q)] \mathcal{V}_{T,\tau_N}(q) \} . \end{aligned} \quad (21)$$

Eq. (19) can be simplified by introducing the functions:

$$\begin{aligned} \mathcal{I}(q_0, \mathbf{q}) &= \frac{-\pi}{(2\pi)^3} \int d\mathbf{h}' \theta(|\mathbf{q}+\mathbf{h}'| - k_F) \theta(k_F - |\mathbf{h}'|) \delta(q_0 - \varepsilon_{\mathbf{h}'+\mathbf{q}} + \varepsilon_{\mathbf{h}}) , \\ \mathcal{R}(q_0, \mathbf{q}) &= \frac{1}{(2\pi)^3} \mathcal{P} \int d\mathbf{h} \frac{\theta(|\mathbf{q}-\mathbf{h}| - k_F) \theta(k_F - |\mathbf{h}|)}{q_0 - (\varepsilon_{\mathbf{h}-\mathbf{q}} - \varepsilon_{\mathbf{h}})} , \end{aligned} \quad (22)$$

where $\mathcal{I}(q_0, \mathbf{q})$ is the imaginary part of the Lindhard function and the explicit expression for $\mathcal{R}(q_0, \mathbf{q})$ is given in Appendix B. Therefore:

$$\begin{aligned} \Gamma_{\tau_{\Lambda'}\tau_{\Lambda}\tau_N}^{DDD}(\mathbf{k}, k_F) &= -\frac{\mathcal{N}^2(k_F)}{(2\pi)^3} (G_F m_\pi^2)^2 \frac{f_\pi^2}{m_\pi^2} \int d\mathbf{q} \theta(q_0) \theta(|\mathbf{k} - \mathbf{q}| - k_F) \\ &\times \{ [S'_{\tau_{\Lambda'}}(q) S'_{\tau_{\Lambda}}(q) + P_{C,\tau_{\Lambda'}}(q) P_{C,\tau_{\Lambda}}(q)] \mathcal{V}_{C,\tau_N}(q) \\ &+ [S_{\tau_{\Lambda'}}(q) S_{\tau_{\Lambda}}(q) + P_{L,\tau_{\Lambda'}}(q) P_{L,\tau_{\Lambda}}(q)] \mathcal{V}_{L,\tau_N}(q) \\ &+ 2 [S_{V,\tau_{\Lambda'}}(q) S_{V,\tau_{\Lambda}}(q) + P_{T,\tau_{\Lambda'}}(q) P_{T,\tau_{\Lambda}}(q)] \mathcal{V}_{T,\tau_N}(q) \} \\ &\times \mathcal{R}(-q_0, \mathbf{q}) \mathcal{I}(q_0, \mathbf{q}) . \end{aligned} \quad (23)$$

Then one has to perform the isospin summation to obtain

$$\Gamma_{n(p)}^{DDD}(\mathbf{k}, k_F) = \sum_{\tau_{\Lambda'}, \tau_{\Lambda}, \tau_N=0,1} \mathcal{T}_{\tau_{\Lambda'}\tau_{\Lambda}\tau_N, n(p)}^{PQQ'} \Gamma_{\tau_{\Lambda'}\tau_{\Lambda}\tau_N}^{DDD}(\mathbf{k}, k_F) . \quad (24)$$

The final result obtained after the local density approximation is therefore:

$$\begin{aligned} \Gamma_n^{DDD} &= 2\{\Gamma_{111}^{DDD} + \Gamma_{000}^{DDD} + \Gamma_{010}^{DDD} + \Gamma_{101}^{DDD}\} , \\ \Gamma_p^{DDD} &= 2\{5\Gamma_{111}^{DDD} + \Gamma_{000}^{DDD} - \Gamma_{010}^{DDD} - \Gamma_{101}^{DDD}\} . \end{aligned} \quad (25)$$

Finally, we present the partial rates corresponding to the diagram $DDDD$ of Fig. 7. By applying the same procedure used for $\Gamma_{\tau_{\Lambda'}\tau_{\Lambda}\tau_N}^{DDD}$ to Eq. (17) we obtain:

$$\begin{aligned} \Gamma_{\tau_{N'}\tau_{\Lambda'}\tau_{\Lambda}\tau_N}^{DDDD}(\mathbf{k}, k_F) &= -\frac{\mathcal{N}^2(k_F)}{(2\pi)^2} (G_F m_\pi^2)^2 \left(\frac{f_\pi^2}{m_\pi^2}\right)^2 \int d\mathbf{q} \theta(q_0) \\ &\times \theta(|\mathbf{k} - \mathbf{q}| - k_F) \{ (S'_{\tau_{\Lambda'}} S'_{\tau_{\Lambda}} + P_{C,\tau_{\Lambda'}} P_{C,\tau_{\Lambda}}) \mathcal{V}_{C,\tau_N}^2 \\ &+ (S_{\tau_{\Lambda'}} S_{\tau_{\Lambda}} + P_{L,\tau_{\Lambda'}} P_{L,\tau_{\Lambda}}) \mathcal{V}_{L,\tau_N}^2 \\ &+ 2 (S_{V,\tau_{\Lambda'}} S_{V,\tau_{\Lambda}} + P_{T,\tau_{\Lambda'}} P_{T,\tau_{\Lambda}}) \mathcal{V}_{T,\tau_N}^2 \} \\ &\times \mathcal{R}^2(-q_0, \mathbf{q}) \mathcal{I}(q_0, \mathbf{q}) , \end{aligned} \quad (26)$$

and

$$\begin{aligned} \Gamma_n^{DDDD} &= 4\{\Gamma_{1111}^{DDD} + \Gamma_{0000}^{DDD} + \Gamma_{0101}^{DDD} + \Gamma_{1010}^{DDD}\} , \\ \Gamma_p^{DDDD} &= 4\{5\Gamma_{1111}^{DDD} + \Gamma_{0000}^{DDD} - \Gamma_{0101}^{DDD} - \Gamma_{1010}^{DDD}\} , \end{aligned} \quad (27)$$

after performing the local density approximation.

In this paper the $\Gamma_{n(p)}^{P'PQQ'}$ exchange terms will be neglected. Indeed, from our numerical results discussed in the next Section it turns out that already the direct contribution $\Gamma_{n(p)}^{DDDD}$

is small and approximately one order of magnitude smaller than $\Gamma_{n(p)}^{DDDD}$. Moreover, according to the results obtained for the $\Gamma_{n(p)}^{PQQ'}$'s, $P'PQQ'$ exchange contributions are expected to be even smaller than the direct term $DDDD$.

VI. RESULTS

In the previous Section we have seen how the neutron- and proton-induced decay widths can be written in the form:

$$\begin{aligned} \Gamma_{n(p)} &= \Gamma_{n(p)}^0 + \Gamma_{n(p)}^{0\text{-GSC}} + \Gamma_{n(p)}^{\text{GSC}} \\ &\equiv \sum_{P,Q=D,E} \Gamma_{n(p)}^{PQ} + \sum_{P,Q,Q'=D,E} \Gamma_{n(p)}^{PQQ'} + \sum_{P',P,Q,Q'=D,E} \Gamma_{n(p)}^{P'PQQ'} , \end{aligned} \quad (28)$$

$\Gamma_{n(p)}^0$ being the rates obtained for an uncorrelated hypernuclear ground state, $\Gamma_{n(p)}^{\text{GSC}}$ the rates originated by ground state correlations and $\Gamma_{n(p)}^{0\text{-GSC}}$ the rates resulting from the interference between uncorrelated and correlated ground states.

For the present scheme containing the transition amplitudes (a) and (b1) of Fig. 3, where antisymmetrization is considered for the weak transition potential $V^{\Lambda N \rightarrow NN}$ and the nuclear residual interaction V^{NN} , we obtained: two contributions to $\Gamma_{n(p)}^0$, which are $\Gamma_{n(p)}^{DD} = \Gamma_{n(p)}^{EE}$ and $\Gamma_{n(p)}^{DE} = \Gamma_{n(p)}^{ED}$ and are generated by the square of amplitude (a); eight different $\Gamma_{n(p)}^{PQQ'}$ contributions to $\Gamma_{n(p)}^{0\text{-GSC}}$, which are interferences between the (a) and (b1) amplitudes; sixteen different $\Gamma_{n(p)}^{P'PQQ'}$ contributions to $\Gamma_{n(p)}^{\text{GSC}}$, which originate from the square of amplitude (b1). An early evaluation of $\Gamma_{n(p)}^0$ has been performed in Ref. [12], while $\Gamma_{n(p)}^{0\text{-GSC}}$ and $\Gamma_{n(p)}^{\text{GSC}}$ are discussed here for the first time. Among the $\Gamma_{n(p)}^{P'PQQ'}$'s, here we only calculate the direct terms $\Gamma_{n(p)}^{DDDD}$.

A. ${}_{\Lambda}^{12}\text{C}$

We start by discussing the relevance of the Pauli exchange terms in $\Gamma_{n(p)}^0$ and $\Gamma_{n(p)}^{0\text{-GSC}}$. Our results for Γ_n^{PQ} and Γ_p^{PQ} are given in Table I for the decay of ${}_{\Lambda}^{12}\text{C}$. Note that, for symmetry, $\Gamma_{n(p)}^0$ are twice the sum of $\Gamma_{n(p)}^{DD}$ and $\Gamma_{n(p)}^{DE}$. Exchange terms contribute to the uncorrelated rates for neutron-induced (proton-induced) decays by 5.1% (0.3%). Thus, they tend to increase Γ_n/Γ_p while having a very small effect on Γ_1 .

TABLE I: Direct and exchange Γ_n^{PQ} and Γ_p^{PQ} terms for ^{12}C in units of the free Λ decay rate, $\Gamma^0 = 2.52 \cdot 10^{-6}$ eV. The first column indicates the two different isospin channels and their sum. Note that $\Gamma_{n(p)}^{DD} = \Gamma_{n(p)}^{EE}$ and $\Gamma_{n(p)}^{DE} = \Gamma_{n(p)}^{ED}$.

Channel	$2\Gamma^{DD}$	$2\Gamma^{DE}$	Γ^0
$\Lambda n \rightarrow nn$	0.146	0.008	0.154
$\Lambda p \rightarrow np$	0.469	0.002	0.470
sum	0.615	0.009	0.624

In Table II we present predictions for the $\Gamma_n^{PQQ'}$ and $\Gamma_p^{PQQ'}$ contributions derived from the Goldstone diagrams of Fig. 8, again for ^{12}C . As expected, the direct terms Γ_n^{DDD} and Γ_p^{DDD} are the main contributions. Nevertheless, the effect of antisymmetry on the two isospin channels is significant: it increases $\Gamma_n^{0\text{-GSC}}$ by 34% while decreasing $\Gamma_p^{0\text{-GSC}}$ by 8%. The overall effect on $\Gamma_1^{0\text{-GSC}} = \Gamma_n^{0\text{-GSC}} + \Gamma_p^{0\text{-GSC}}$ is a very small increase, of 2%. We note that, with topologically equivalent diagrams, in Ref. [21] a similar quasi-cancellation between neutron- and proton-induced decays has been found in nucleon spectra calculations. Moreover, in Ref. [19] it has been shown that the evaluation of the GSC exchange terms is important for the rate Γ_2 as well. We emphasize that the exact evaluation of exchange diagrams has been mostly ignored in the literature. It is usually a quite involved (but necessary) task, given the rapidly increasing number of terms one has to consider when going to higher orders in the nuclear residual interaction. Unfortunately, there is no general rule to anticipate the need for the evaluation of exchange terms when the corresponding direct contribution is important.

In Table III we present the different contributions to the rates Γ_n and Γ_p of Eq. (28). The uncorrelated parts Γ_n^0 and Γ_p^0 dominate over the remaining ones: $\Gamma_1^0 = \Gamma_n^0 + \Gamma_p^0$ constitutes the 86% of the total Γ_1 . Then, $\Gamma_1^{0\text{-GSC}} = \Gamma_n^{0\text{-GSC}} + \Gamma_p^{0\text{-GSC}}$ and $\Gamma_1^{\text{GSC}} = \Gamma_n^{\text{GSC}} + \Gamma_p^{\text{GSC}}$ represent 13% and 1% of Γ_1 , respectively. We remind the reader that $\Gamma_{n(p)}^{\text{GSC}}$ are calculated from the direct diagram $DDDD$ in Fig. 7, while $P'PQQ'$ exchange terms are neglected. This omission is justified by the smallness of the direct contributions $\Gamma_{n(p)}^{DDDD}$: the neglected exchange part of Γ_1^{GSC} should contribute to Γ_1 by less than 1%. Thus, a challenging calculation of the fifteen $P'PQQ'$ exchange diagrams can be reasonably avoided.

TABLE II: Direct and exchange $\Gamma_n^{PQQ'}$ and $\Gamma_p^{PQQ'}$ terms for ${}^{12}_\Lambda\text{C}$ obtained from the diagrams of Fig. 8. The first column indicates the two different isospin channels and their sum.

Channel	Γ^{DDD}	Γ^{DDE}	Γ^{DED}	Γ^{EDD}	
$\Lambda n \rightarrow nn$	0.022	-0.002	-0.009	-0.004	
$\Lambda p \rightarrow np$	0.071	0.005	-0.027	-0.011	
sum	0.093	0.003	-0.036	-0.015	
Channel	Γ^{DEE}	Γ^{EDE}	Γ^{EED}	Γ^{EEE}	$\Gamma^0\text{-GSC}$
$\Lambda n \rightarrow nn$	0.006	0.008	0.006	0.002	0.029
$\Lambda p \rightarrow np$	-0.008	0.009	0.025	0.002	0.066
sum	-0.003	0.017	0.031	0.004	0.095

TABLE III: Predictions for the one-nucleon induced decay rates of Eq. (28) for ${}^{12}_\Lambda\text{C}$. The first column indicates the two different isospin channels and their sum.

Channel	Γ^0	$\Gamma^0\text{-GSC}$	Γ^{GSC}	Γ
$\Lambda n \rightarrow nn$	0.154	0.029	0.002	0.185
$\Lambda p \rightarrow np$	0.470	0.066	0.008	0.544
sum	0.624	0.095	0.010	0.729

Our predictions for the one- and two-nucleon induced decay rates for ${}^{12}_\Lambda\text{C}$ are given in Table IV and compared with the most recent data by KEK [26] and FINUDA [27]. For completeness, we report results without and with the inclusion of antisymmetrization and GSC. It should be noted that the hypernuclear ground state normalization function $\mathcal{N}(k_F)$ of Eq. (5) equally affects Γ_1 and Γ_2 . This function is not identically equal to one only when GSC are present. Therefore, the Γ_1 result without GSC and with exchange terms of Table IV, 0.74, is bigger than the prediction for Γ_1^0 of Table III, 0.62, which has been obtained instead by including both GSC and antisymmetrization in the normalization function. This comparison gives an idea of the importance of a proper normalization of the hypernuclear ground state. GSC produces a sizable increase in the value of Γ_{NM} , thanks to the opening of the two-nucleon induced channel, while Γ_1 remains practically unaffected. The effect of GSC

on the Γ_n/Γ_p ratio is a small increase of 4%, which is due entirely to the exchange terms in $\Gamma_n^{0\text{-GSC}}$ and $\Gamma_p^{0\text{-GSC}}$ (see Table II). Antisymmetrization on the contrary introduce an increase of Γ_1 and a reduction of Γ_2 , and as a result a sizable reduction of Γ_2/Γ_1 . We conclude that GSC are important to get agreement with data on Γ_{NM} , while antisymmetrization is crucial to reproduce the data for Γ_2/Γ_1 . Note indeed that only with the set of results including both exchange terms and GSC we can achieve an overall agreement with all data.

TABLE IV: The non-mesonic weak decay widths of $^{12}_{\Lambda}\text{C}$. Results are given without and with the contributions of antisymmetrization and ground state correlations. The most recent data, from KEK [26] and FINUDA [27], are given for comparison.

Ant./GSC	Γ_n	Γ_p	Γ_1	Γ_2	Γ_{NM}	Γ_n/Γ_p	$\Gamma_2/\Gamma_{\text{NM}}$
no/no	0.15	0.47	0.62	0	0.62	0.31	0
yes/no	0.18	0.56	0.74	0	0.74	0.33	0
no/yes	0.15	0.47	0.61	0.31	0.91	0.31	0.50
yes/yes	0.19	0.55	0.73	0.25	0.98	0.34	0.26
KEK	0.23 ± 0.08	0.45 ± 0.10	0.68 ± 0.13	0.27 ± 0.13	0.95 ± 0.04	$0.51 \pm 0.13 \pm 0.05$	0.29 ± 0.13
FINUDA							0.24 ± 0.10

Despite this agreement, we have to admit that more refined and systematic theoretical studies should be performed before one can reach definite conclusions from the comparison between theory and experiment. For instance, the result obtained for Γ_{NM} requires a comment on the eventual inclusion of the full set of diagrams stemming from the amplitudes in Figs. 3 and 4 and eventually from other amplitudes. At first glance, one may think that the final outcome from all these diagrams would be a bigger value for Γ_{NM} , thus spoiling the good agreement with data of the present result. This is not necessarily the case, for two reasons. First, the amplitudes (*d1*) and (*d2*) in Fig. 3 and the amplitude (*c*) in Fig. 4 originate from $1\Delta 1p2h$ GSC. The inclusion of these correlation amplitudes requires the introduction of new terms in the ground state normalization function (5); this leads to a reduction of the individual values for each decay width, including the ones we have obtained above. From the previous studies in Refs. [18, 19] one observes the following property, introduced by ground state normalization: a certain redistribution of the total non-mesonic decay strength among

the partial contributions occurs when new self-energy terms are included. Secondly, the presence of several additional self-energy diagrams which are interference terms between amplitudes could also bring to a reduction of the decay rates Γ_1 and Γ_2 .

B. Medium and heavy hypernuclei

In order to have a further indication of the reliability of our framework, which adopts the local density approximation to obtain results for finite hypernuclei, we have extended the calculation to medium and heavy Λ hypernuclei. All the GSC contributions and the antisymmetrization terms discussed in detail for ${}^{12}_{\Lambda}\text{C}$ have been taken into account. The results we have obtained are given in Table V and are compared with recent data in Figure 9.

The GSC-free rate Γ_1^0 represents 86% of the rate $\Gamma_1 = \Gamma_1^0 + \Gamma_1^{0-\text{GSC}} + \Gamma_1^{\text{GSC}}$ for ${}^{12}_{\Lambda}\text{C}$. For increasing hypernuclear mass number A , this contribution decreases and reaches 81% for ${}^{208}_{\Lambda}\text{Pb}$. As expected, GSC contributions are thus more important for heavy hypernuclei.

The one- and two-nucleon induced rates increase with A and rapidly saturate. Saturation is expected to begin for those hypernuclei whose radius becomes sensitively larger than the range of the non-mesonic processes. The fact that for ${}^{40}_{\Lambda}\text{Ca}$ and ${}^{208}_{\Lambda}\text{Pb}$ we obtain very similar predictions informs us that in ${}^{208}_{\Lambda}\text{Pb}$ the non-mesonic decay (both one- and two-nucleon stimulated) involve the same nucleon shells which participate in the decay of ${}^{40}_{\Lambda}\text{Ca}$. Indeed, the Λ wave function (s level of the Λ -nucleus mean potential) is well overlapped to the hypernuclear core already in ${}^{40}_{\Lambda}\text{Ca}$.

It should be noted that the slight decrease of the non-mesonic rate Γ_{NM} going from ${}^{89}_{\Lambda}\text{Y}$ to ${}^{139}_{\Lambda}\text{La}$ is due to the special value of the oscillator parameter $\hbar\omega$ adopted for this hypernucleus. Such a parameter, which is obtained as the difference between the measured s and p Λ energy levels in ${}^{139}_{\Lambda}\text{La}$, is indeed smaller than the values measured for the two neighboring hypernuclei of our calculation, ${}^{89}_{\Lambda}\text{Y}$ and ${}^{208}_{\Lambda}\text{Pb}$.

The contribution of the two-nucleon induced width is almost independent of the hypernuclear mass number and oscillates between 22 and 26% of Γ_{NM} . We note from Figure 9 that the datum recently determined at KEK, $\Gamma_2 = 0.27 \pm 0.13$ [26], is well reproduced by our calculation. Also the recent determination obtained by FINUDA [27] of $\Gamma_2/\Gamma_{\text{NM}} = 0.22 \pm 0.08$ for hypernuclei from ${}^5_{\Lambda}\text{He}$ to ${}^{16}_{\Lambda}\text{O}$ is in agreement with our predictions.

Concerning Γ_{NM} , the agreement of our predictions with data is also rather good. The

only exception is the large underestimation of the datum for the $A \simeq 200$ region, which however is also difficult to reconcile with the decay rate measured at KEK for ${}_{\Lambda}^{56}\text{Fe}$. No known mechanism can be responsible for a large increase in the non-mesonic decay rate when going from ${}_{\Lambda}^{56}\text{Fe}$ to the $A \simeq 200$ region. Concerning the datum for $A \simeq 200$, we have to note that, given the difficulty in employing direct timing methods for heavy hypernuclei, it has been obtained in experiments (performed at COSY, Juelich [28]) which measured the fission fragments (which are supposed to be generated by the non-mesonic decay) emitted by hypernuclei produced in proton-nucleus reactions. Large uncertainties affect such delayed fission experiments, because of the limited precision of the employed recoil shadow method. The produced hypernuclei cannot be unambiguously identified with this method. It is also possible that mechanisms other than the non-mesonic decay contributed to hypernuclear fission in these experiments. The datum reported in Figure 9 has been obtained as an average from measurements for hypernuclei produced in proton-Au, proton-Bi and proton-U reactions.

TABLE V: Decay rates predicted for medium to heavy hypernuclei.

Hypernucleus	Γ_1^0	Γ_1	Γ_2	Γ_{NM}
${}_{\Lambda}^{11}\text{B}$	0.56	0.64	0.18	0.82
${}_{\Lambda}^{12}\text{C}$	0.62	0.73	0.25	0.98
${}_{\Lambda}^{27}\text{Al}$	0.80	0.94	0.28	1.22
${}_{\Lambda}^{28}\text{Si}$	0.81	0.96	0.29	1.25
${}_{\Lambda}^{40}\text{Ca}$	0.87	1.03	0.29	1.33
${}_{\Lambda}^{56}\text{Fe}$	0.88	1.06	0.33	1.39
${}_{\Lambda}^{89}\text{Y}$	0.87	1.06	0.33	1.39
${}_{\Lambda}^{139}\text{La}$	0.86	1.04	0.32	1.36
${}_{\Lambda}^{208}\text{Pb}$	0.86	1.06	0.34	1.40

We think that the results of the evaluation for medium and heavy hypernuclei are encouraging: they give us some confidence in using the local density approximation for obtaining results in finite hypernuclei, even in light systems such as ${}_{\Lambda}^{12}\text{C}$.

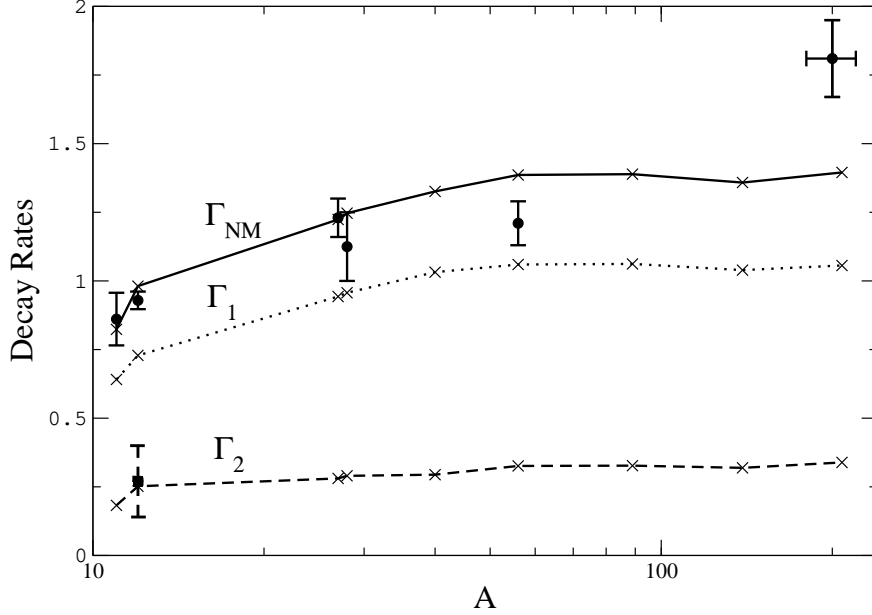


FIG. 9: The predictions for the decay rates Γ_1 , Γ_2 and $\Gamma_{\text{NM}} = \Gamma_1 + \Gamma_2$ are given as a function of the hypernuclear mass number A . The results for Γ_{NM} are compared with experimental data for ${}^{11}_{\Lambda}\text{B}$ [29], ${}^{12}_{\Lambda}\text{C}$ [30], ${}^{27}_{\Lambda}\text{Al}$ [29], ${}^{28}_{\Lambda}\text{Si}$ [29], ${}^{56}_{\Lambda}\text{Fe}$ [29] and for the region of A between 180 and 220 [28]. The datum for Γ_2 is from Ref. [26].

C. Closing remarks

Before concluding, we make here some further comments on our calculation. Through our work we wish to emphasize the importance of a detailed many-body treatment of non-mesonic decay. This requires the identification and evaluations of a large number of diagrams, working on a step-by-step basis with the perspective of reaching the condition in which the terms that are not taken into account can be safely neglected. Considering the evolution in the predictions obtained in recent works (see especially Refs. [18, 19]) and here, this stability of results has not been achieved yet, and new many-body terms must be considered. In our opinion, one should explore the dependencies of predictions on the weak transition potential model only after these complicated many-body aspects are properly understood. Finally, one should attempt to reach a detailed agreement with experiment for Γ_{NM} , Γ_n/Γ_p and $\Gamma_2/\Gamma_{\text{NM}}$ and thus extract sensible information on strangeness-changing baryon interactions. From the experimental side, new and improved data are expected from FINUDA@Daphne [31], JPARC [32, 33] and GSI [34]. A direct experimental identification

of the two–nucleon induced channels together with the measurement of Γ_2 is a question of particular importance.

We end this Section with a comment to emphasize the importance of evaluating exchange terms. In our many–body inspired calculation, such terms are considered together with GSC contributions, which are included on the same ground for one– and two–nucleon induced decays. GSC and exchange terms improve by 10% the value of Γ_n/Γ_p . Once GSC are included, antisymmetrization turns out to be particularly important for both the one– and the two–nucleon induced channels, reducing Γ_2 by 18% and increasing Γ_1 by 20%. It would thus be pointless to neglect exchange terms and evaluate only direct ones. Although the introduction of antisymmetry is a difficult task in a many–body framework, one should evaluate all those exchange diagrams which are companions of a direct diagram which one knows to be relevant.

VII. CONCLUSIONS

In this contribution we have studied the effects of GSC in the non–mesonic weak decay of Λ hypernuclei. A non–relativistic nuclear matter scheme has been adopted together with the local density approximation, for calculations in hypernuclei ranging from ${}^{\Lambda}_{11}\text{B}$ to ${}^{\Lambda}_{208}\text{Pb}$. All isospin channels contributing to one– and two–nucleon induced decays have been considered. The employed weak transition potential contains the exchange of mesons of the pseudoscalar and vector octets, π , η , K , ρ , ω and K^* . The residual strong interaction, responsible for GSC, has been modeled on a Bonn potential based on π –, ρ –, σ – and ω –exchange.

By using the Goldstone diagrams technique, GSC have been introduced on the same footing for one– and two–nucleon stimulated decays. The normalization of the hypernuclear ground state introduced by GSC has been taken into account. We have devoted particular attention to those GSC affecting the decay widths Γ_n and Γ_p . The many–body Λ self–energy terms we have considered are originated by the transition amplitudes (a) and (b1) of Fig. 3 (for one–nucleon induced decays) and by the amplitude (a) of Fig. 4 (for two–nucleon induced decays). Our approach embodies fermion antisymmetry, i.e., both direct and exchange interactions are considered in the various diagrams. Concerning one–nucleon induced decays, we have evaluated GSC–free rates $\Gamma_{n(p)}^0$, generated by amplitude (a), purely GSC terms $\Gamma_{n(p)}^{\text{GSC}}$, produced by amplitude (b1), and interference terms $\Gamma_{n(p)}^{0-\text{GSC}}$ between uncorrelated and

correlated hypernuclear ground states, i.e., between amplitudes (a) and (b1).

The dominant contribution to $\Gamma_1 = \Gamma_1^0 + \Gamma_1^{0-\text{GSC}} + \Gamma_1^{\text{GSC}}$ turned out to be $\Gamma_1^0 = \Gamma_n^0 + \Gamma_p^0$. For ${}^{12}_\Lambda\text{C}$, $\Gamma_1^{0-\text{GSC}} = \Gamma_n^{0-\text{GSC}} + \Gamma_p^{0-\text{GSC}}$ and $\Gamma_1^{\text{GSC}} = \Gamma_n^{\text{GSC}} + \Gamma_p^{\text{GSC}}$ represented 13% and 1% of the rate Γ_1 , respectively; GSC are thus responsible for 14% of the one-nucleon induced width (such contribution increases up to 19% for ${}^{208}_\Lambda\text{Pb}$). The above results justify the fact that we have neglected the exchange terms in $\Gamma_{n(p)}^{\text{GSC}}$. Exchange contributions are rather relevant in the calculation of $\Gamma_{n(p)}^{0-\text{GSC}}$ (for ${}^{12}_\Lambda\text{C}$, they increase $\Gamma_n^{0-\text{GSC}}$ by 34% and decrease $\Gamma_p^{0-\text{GSC}}$ by 8%), while only scarcely contribute to $\Gamma_{n(p)}^0$. GSC and exchange terms together increase the value of Γ_n/Γ_p for ${}^{12}_\Lambda\text{C}$ by 10%. Thanks to the opening of the two-nucleon induced channel, GSC produces a sizable increase (of 32% for ${}^{12}_\Lambda\text{C}$ when exchange terms are included) in the value of $\Gamma_{\text{NM}} = \Gamma_1 + \Gamma_2$.

The agreement among our final results and recent data is quite good and clearly demonstrates the necessity of including GSC and antisymmetrization effects. Nevertheless, we believe that a refinement of the present scheme must be pursued. Additional many-body terms should be considered, involving for instance the $\Delta(1232)$ resonance. Only after a certain stability of predictions is reached within such a microscopic approach one should explore the dependencies on the weak transition potential model and determine, through detailed comparison with experiment, sensible information on strangeness-changing baryon interactions.

Acknowledgments

This work has been partially supported by the CONICET, under contract PIP 6159. This Research is part of the EU Initiative FP7-Project HadronPhysics2 under Project number 227431. We would like to thank A. Ramos and F. Krmpotic for the helpful discussion and the careful reading of the manuscript.

Appendix A

In this Appendix we present explicit expressions for the decay rates $\Gamma_{n(p)}^{PQQ'}$ with $PQQ' \neq DDD$ associated to the Goldstone diagrams of Fig. 8 and contributing to Eq. (14). In the

main text, these widths have been written as:

$$\Gamma_{n(p)}^{PQQ'} = \sum_{\tau_{\Lambda'}, \tau_{\Lambda}, \tau_N=0,1} \mathcal{T}_{\tau_{\Lambda'}, \tau_{\Lambda}, \tau_N, n(p)}^{PQQ'} \Gamma_{\tau_{\Lambda'}, \tau_{\Lambda}, \tau_N}^{PQQ'}(\mathbf{k}, k_F), \quad (29)$$

where

$$\begin{aligned} \Gamma_{\tau_{\Lambda'}, \tau_{\Lambda}, \tau_N}^{PQQ'}(\mathbf{k}, k_F) &= \mathcal{N}^2(k_F) \frac{1}{4} \frac{(-1)^n}{(2\pi)^8} (G_F m_\pi^2)^2 \frac{f_\pi^2}{m_\pi^2} \\ &\times \int \int \int d\mathbf{q} d\mathbf{h} d\mathbf{h}' \mathcal{W}_{\tau_{\Lambda'}, \tau_{\Lambda}, \tau_N}^{PQQ'}(q, q', t) \\ &\times \Theta(k, q, q', t, h, h', k_F) \frac{1}{\varepsilon_{2p2h}^{PQQ'}} \delta(q_0 - (\varepsilon_{\mathbf{h}'+\mathbf{q}} - \varepsilon_{\mathbf{h}'})). \end{aligned} \quad (30)$$

The isospin index τ_Λ ($\tau_{\Lambda'}$) of the weak transition potential is associated to an energy–momentum q (q'), while the nuclear strong interaction isospin index is τ_N and the corresponding energy–momentum t . In the following subsections we give the functions $\mathcal{W}_{\tau_{\Lambda'}, \tau_{\Lambda}, \tau_N}^{PQQ'}(q, q', t)$ and $\Theta(k, q, q', t, h, h', k_F)$, the energy denominator $\varepsilon_{2p2h}^{PQQ'}$ and n (the number of crossing between fermionic lines) for the various cases. Finally, we show the isospin sums of Eq. (29).

i) $\Gamma_{\mathbf{n}(\mathbf{p})}^{DDE}$

The $\mathcal{W}_{\tau_{\Lambda'}, \tau_{\Lambda}, \tau_N}^{DDE}(q, q', t)$ function, where $q' = q$ and $t = h' - h + q$, is identical to the $\mathcal{S}_{\tau' \tau_N \tau}^{ded}(q, q', t)$ function in Eq. (A.1) of Ref. [21]. Moreover:

$$\begin{aligned} \Theta(k, q, q', t, h, h', k_F) &= \theta(q_0) \theta(|\mathbf{k} - \mathbf{q}| - k_F) \theta(|\mathbf{q} - \mathbf{h}| - k_F) \\ &\times \theta(k_F - |\mathbf{h}|) \theta(|\mathbf{q} + \mathbf{h}'| - k_F) \theta(k_F - |\mathbf{h}'|), \end{aligned} \quad (31)$$

$$\varepsilon_{2p2h}^{DDE} = \varepsilon_{2p2h}^{DDD} \equiv k_0 - \varepsilon_{\mathbf{k}-\mathbf{q}} + \varepsilon_{\mathbf{h}-\mathbf{q}} - \varepsilon_{\mathbf{h}} - V_N, \quad (32)$$

and $n = 0$. The isospin sums are given by:

$$\begin{aligned} \Gamma_n^{DDE} &= -\Gamma_{111}^{DDE} + \Gamma_{000}^{DDE} + 3\Gamma_{101}^{DDE} + \Gamma_{110}^{DDE} - \Gamma_{011}^{DDE} + \Gamma_{100}^{DDE} \\ &\quad + 3\Gamma_{001}^{DDE} + \Gamma_{010}^{DDE}, \\ \Gamma_p^{DDE} &= -5\Gamma_{111}^{DDE} + \Gamma_{000}^{DDE} - 3\Gamma_{101}^{DDE} + 5\Gamma_{110}^{DDE} + \Gamma_{011}^{DDE} - \Gamma_{100}^{DDE} \\ &\quad + 3\Gamma_{001}^{DDE} - \Gamma_{010}^{DDE}. \end{aligned}$$

ii) $\Gamma_{\mathbf{n}(\mathbf{p})}^{DED}$

The $\mathcal{W}_{\tau_N \tau_A \tau_N}^{DED}(q, q', t)$ function, where $q' = k - h$ and $t = q$, is identical to the $\mathcal{S}_{\tau' \tau_N \tau}^{dde}(q, q', t)$ function in Eq. (A.3) of Ref. [21]. Moreover:

$$\Theta(k, q, q', t, h, h', k_F) = \theta(q_0) \theta(|\mathbf{k} - \mathbf{q}| - k_F) \theta(|\mathbf{q} - \mathbf{h}| - k_F) \quad (33)$$

$$\times \theta(k_F - |\mathbf{h}|) \theta(|\mathbf{q} + \mathbf{h}'| - k_F) \theta(k_F - |\mathbf{h}'|) ,$$

$$\varepsilon_{2p2h}^{DED} = \varepsilon_{2p2h}^{DDD} , \quad (34)$$

and $n = 0$. The isospin sums are given by:

$$\Gamma_n^{DED} = -\Gamma_{111}^{DED} + \Gamma_{000}^{DED} + \Gamma_{101}^{DED} + 3\Gamma_{110}^{DED} - \Gamma_{011}^{DED} + \Gamma_{100}^{DED}$$

$$+ 3\Gamma_{001}^{DED} + 3\Gamma_{010}^{DED} ,$$

$$\Gamma_p^{DED} = -5\Gamma_{111}^{DED} + \Gamma_{000}^{DED} + 5\Gamma_{101}^{DED} - 3\Gamma_{110}^{DED} + \Gamma_{011}^{DED} - \Gamma_{100}^{DED}$$

$$- \Gamma_{001}^{DED} + 3\Gamma_{010}^{DED} .$$

iii) $\Gamma_{\mathbf{n}(\mathbf{p})}^{EDD}$

The $\mathcal{W}_{\tau_N \tau_A \tau_N}^{EDD}(q, q', t)$ function, where $q' = k - q - h'$ and $t = q$, is identical to the $\mathcal{S}_{\tau' \tau_N \tau}^{dde}(q, q', t)$ function in Eq. (A.3) of Ref. [21]. Moreover:

$$\Theta(k, q, q', t, h, h', k_F) = \theta(q_0) \theta(|\mathbf{k} - \mathbf{q}| - k_F) \theta(|\mathbf{q} - \mathbf{h}| - k_F) \quad (35)$$

$$\times \theta(k_F - |\mathbf{h}|) \theta(|\mathbf{q} + \mathbf{h}'| - k_F) \theta(k_F - |\mathbf{h}'|) ,$$

$$\varepsilon_{2p2h}^{EDD} = \varepsilon_{2p2h}^{DDD} , \quad (36)$$

and $n = 1$. The isospin sums are given by:

$$\Gamma_n^{EDD} = -\Gamma_{111}^{EDD} + \Gamma_{000}^{EDD} - \Gamma_{101}^{EDD} + 3\Gamma_{110}^{EDD} + \Gamma_{011}^{EDD} + 3\Gamma_{100}^{EDD}$$

$$+ \Gamma_{001}^{EDD} + \Gamma_{010}^{EDD} ,$$

$$\Gamma_p^{EDD} = -5\Gamma_{111}^{EDD} + \Gamma_{000}^{EDD} + \Gamma_{101}^{EDD} - 3\Gamma_{110}^{EDD} + 5\Gamma_{011}^{EDD} + 3\Gamma_{100}^{EDD}$$

$$- \Gamma_{001}^{EDD} - \Gamma_{010}^{EDD} .$$

iv) $\Gamma_{\mathbf{n}(\mathbf{p})}^{DEE}$

The $\mathcal{W}_{\tau_{\Lambda'}\tau_{\Lambda}\tau_N}^{DEE}(q, q', t)$ function, where $q' = k - h$ and $t = h - h' - q$, is identical to the $\mathcal{S}_{\tau'\tau_N\tau}^{eed}(q, q', t)$ function in Eq. (A.7) of Ref. [21]. Moreover:

$$\begin{aligned} \Theta(k, q, q', t, h, h', k_F) &= \theta(q_0)\theta(|\mathbf{k} - \mathbf{q}| - k_F)\theta(|\mathbf{q} - \mathbf{h}| - k_F) \\ &\times \theta(k_F - |\mathbf{h}|)\theta(|\mathbf{q} + \mathbf{h}'| - k_F)\theta(k_F - |\mathbf{h}'|) , \end{aligned} \quad (37)$$

$$\varepsilon_{2p2h}^{DEE} = \varepsilon_{2p2h}^{DDD} , \quad (38)$$

and $n = 1$. The isospin sums are given by:

$$\begin{aligned} \Gamma_n^{DEE} &= 5\Gamma_{111}^{DEE} + \Gamma_{000}^{DEE} + \Gamma_{101}^{DEE} + \Gamma_{110}^{DEE} + 5\Gamma_{011}^{DEE} + \Gamma_{100}^{DEE} \\ &\quad + \Gamma_{001}^{DEE} + \Gamma_{010}^{DEE} , \\ \Gamma_p^{DEE} &= -2\Gamma_{111}^{DEE} - 4\Gamma_{101}^{DEE} + 4\Gamma_{110}^{DEE} + 2\Gamma_{011}^{DEE} + 2\Gamma_{100}^{DEE} \\ &\quad + 2\Gamma_{001}^{DEE} + 2\Gamma_{010}^{DEE} . \end{aligned}$$

v) $\Gamma_{\mathbf{n}(\mathbf{p})}^{EDE}$

The $\mathcal{W}_{\tau_{\Lambda'}\tau_{\Lambda}\tau_N}^{EDE}(q, q', t)$ function, where $q' = k - q - h'$ and $t = h' - h + q$, is identical to the $\mathcal{S}_{\tau'\tau_N\tau}^{eed}(q, q', t)$ function in Eq. (A.7) of Ref. [21]. Moreover:

$$\begin{aligned} \Theta(k, q, q', t, h, h', k_F) &= \theta(q_0)\theta(|\mathbf{k} - \mathbf{q}| - k_F)\theta(|\mathbf{q} - \mathbf{h}| - k_F) \\ &\times \theta(k_F - |\mathbf{h}|)\theta(|\mathbf{q} + \mathbf{h}'| - k_F)\theta(k_F - |\mathbf{h}'|) , \end{aligned} \quad (39)$$

$$\varepsilon_{2p2h}^{EDE} = \varepsilon_{2p2h}^{DDD} , \quad (40)$$

and $n = 1$. The isospin sums are given by:

$$\begin{aligned} \Gamma_n^{EDE} &= -\Gamma_{111}^{EDE} + \Gamma_{000}^{EDE} + 3\Gamma_{101}^{EDE} + \Gamma_{110}^{EDE} - \Gamma_{011}^{EDE} + \Gamma_{100}^{EDE} \\ &\quad + 3\Gamma_{001}^{EDE} + \Gamma_{010}^{EDE} \\ \Gamma_p^{EDE} &= 4\Gamma_{111}^{EDE} + 6\Gamma_{101}^{EDE} - 4\Gamma_{110}^{EDE} - 2\Gamma_{011}^{EDE} + 2\Gamma_{100}^{EDE} + 2\Gamma_{010}^{EDE} \end{aligned}$$

vi) $\Gamma_{\mathbf{n}(\mathbf{p})}^{EED}$

The $\mathcal{W}_{\tau_N \tau_\Lambda \tau_N}^{EED}(q, q', t)$ function, where $q' = k - h$ and $t = k - q - h'$, is identical to the $\mathcal{S}_{\tau' \tau_N \tau}^{ede}(q, q', t)$ function in Eq. (A.5) of Ref. [21]. Moreover:

$$\begin{aligned} \Theta(k, q, q', t, h, h', k_F) &= \theta(q_0) \theta(|\mathbf{k} - \mathbf{q}| - k_F) \theta(|\mathbf{q} + \mathbf{h} + \mathbf{h}' - \mathbf{k}| - k_F) \\ &\quad \times \theta(k_F - |\mathbf{h}|) \theta(|\mathbf{q} + \mathbf{h}'| - k_F) \theta(k_F - |\mathbf{h}'|) , \end{aligned} \quad (41)$$

$$\varepsilon_{2p2h}^{EED} = k_0 - \varepsilon_{\mathbf{h}} + \varepsilon_{\mathbf{q}+\mathbf{h}+\mathbf{h}'-\mathbf{k}} - \varepsilon_{\mathbf{q}+\mathbf{h}'} - V_N , \quad (42)$$

and $n = 1$. The isospin sum are given by:

$$\begin{aligned} \Gamma_n^{EED} &= -\Gamma_{111}^{EED} + \Gamma_{000}^{EED} + \Gamma_{101}^{EED} + 3\Gamma_{110}^{EED} - \Gamma_{011}^{EED} + \Gamma_{100}^{EED} , \\ &\quad + \Gamma_{001}^{EED} + 3\Gamma_{010}^{EED} \\ \Gamma_p^{EED} &= 4\Gamma_{111}^{EED} - 4\Gamma_{101}^{EED} + 6\Gamma_{110}^{EED} - 2\Gamma_{011}^{EED} + 2\Gamma_{100}^{EED} + 2\Gamma_{001}^{EED} . \end{aligned}$$

vii) $\Gamma_{\mathbf{n}(\mathbf{p})}^{EEE}$

The $\mathcal{W}_{\tau_N \tau_\Lambda \tau_N}^{EEE}(q, q', t)$ function, where $q' = k - h$ and $t = h + q - k$, is identical to the $\mathcal{S}_{\tau' \tau_N \tau}^{eee}(q, q', t)$ function in Eq. (A.9) of Ref. [21]. Moreover:

$$\begin{aligned} \Theta(k, q, q', t, h, h', k_F) &= \theta(q_0) \theta(|\mathbf{k} - \mathbf{q}| - k_F) \theta(|\mathbf{h}' + \mathbf{q}| - k_F) \\ &\quad \times \theta(k_F - |\mathbf{h}'|) \theta(k_F - |\mathbf{k} - \mathbf{h} + \mathbf{h}'|) \theta(k_F - |\mathbf{h}|) , \end{aligned} \quad (43)$$

$$\varepsilon_{2p2h}^{EEE} = k_0 - \varepsilon_{\mathbf{h}} + \varepsilon_{\mathbf{h}'} - \varepsilon_{\mathbf{k}-\mathbf{h}+\mathbf{h}'} - V_N , \quad (44)$$

and $n = 0$. The isospin sums are given by:

$$\begin{aligned} \Gamma_n^{EEE} &= 5\Gamma_{111}^{EEE} + \Gamma_{000}^{EEE} + \Gamma_{101}^{EEE} + \Gamma_{110}^{EEE} + 5\Gamma_{011}^{EEE} + \Gamma_{100}^{EEE} \\ &\quad + \Gamma_{001}^{EEE} + \Gamma_{010}^{EEE} , \\ \Gamma_p^{EEE} &= 7\Gamma_{111}^{EEE} + \Gamma_{000}^{EEE} + 5\Gamma_{101}^{EEE} + 5\Gamma_{110}^{EEE} + \Gamma_{011}^{EEE} - \Gamma_{100}^{EEE} \\ &\quad - \Gamma_{001}^{EEE} - \Gamma_{010}^{EEE} . \end{aligned}$$

Appendix B

The explicit expressions of the function $\mathcal{R}(q_0, \mathbf{q})$ of Eq. (22) reads:

$$\begin{aligned} \mathcal{R}(q_0, \mathbf{q}) = & \frac{\pi}{(2\pi)^3} \frac{m}{q} \left\{ \frac{m^2}{q^2} \left[2 \left(q_0 - \frac{q^2}{2m} \right) \frac{q}{m} k_F + \left(\left(q_0 - \frac{q^2}{2m} \right)^2 - \frac{q^2}{m^2} k_F^2 \right) \right. \right. \\ & \times \ln \left| \frac{2mq_0 - q^2 - 2qk_F}{2mq_0 - q^2 + 2qk_F} \right| \left. \right] + \theta(2k_F - q) \left[-\frac{m^2}{q^2} \left(2q_0 \frac{q}{m} \left(k_F - \frac{q}{2} \right) \right. \right. \\ & + \left. \left. \left(q_0^2 - \frac{q^2}{m^2} \left(k_F - \frac{q}{2} \right)^2 \right) \ln \left| \frac{2mq_0 + q^2 - 2qk_F}{2mq_0 - q^2 + 2qk_F} \right| \right) + q \left(\frac{q}{4} - k_F \right) \right. \\ & \left. \left. \times \ln \left| \frac{2mq_0 - q^2 + 2qk_F}{2mq_0 + q^2 - 2qk_F} \right| - q_0 m \ln \left| \frac{q_0^2 m^2 - q^2 (k_F - q/2)^2}{m^2 q_0^2} \right| \right] \right\}, \end{aligned}$$

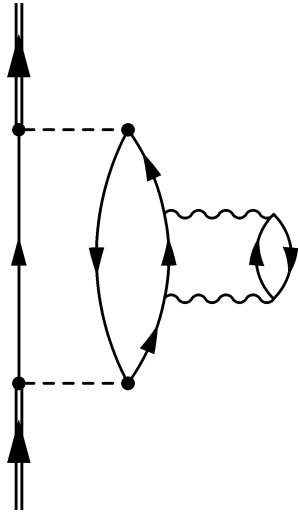
where $q = |\mathbf{q}|$ and m is the nucleon mass.

-
- [1] For a recent collection of reviews on nuclear physics with strangeness see the Special Issue on *Recent Advances in Strangeness Nuclear Physics*, Nucl. Phys. **A 804** (2008) 1.
- [2] E. Oset and A. Ramos, Prog. Part. Nucl. Phys. **41** (1998) 191.
- [3] W. M. Alberico and G. Garbarino, Phys. Rep. **369** (2002) 1; in *Hadron Physics*, IOS Press, Amsterdam, 2005, p. 125. Edited by T. Bressani, A. Filippi and U. Wiedner. Proceedings of the International School of Physics “Enrico Fermi”, Course CLVIII, Varenna (Italy), June 22 – July 2, 2004 [nucl-th/0410059]. For an update of these reviews see Ref. [4].
- [4] C. Chumillas, G. Garbarino, A. Parreño and A. Ramos, Nucl. Phys. **A 804** (2008) 162.
- [5] A. Parreño, Lect. Notes Phys. **724** (2007) 141.
- [6] H. Ota, in *Hadron Physics* (IOS Press, Amsterdam, 2005) p. 219. Edited by T. Bressani, A. Filippi and U. Wiedner. Proceedings of the International School of Physics “Enrico Fermi”, Course CLVIII, Varenna (Italy), June 22 – July 2, 2004.
- [7] J. Nieves and E. Oset, Phys. Rev. **C 47** (1993) 1478; T. Motoba and K. Itonaga, Prog. Theor. Phys. Suppl. **117** (1994) 477; T. Motoba, K. Itonaga and H. Bando, Nucl. Phys. **A 489** (1988) 683.
- [8] A. Gal, Nucl. Phys. **A 828** (2009) 72.
- [9] A. Ramos, M. J. Vicente-Vacas and E. Oset, Phys. Rev. **C 55** (1997) 735; **66** (2002) 039903(E).
- [10] G. Garbarino, A. Parreño and A. Ramos, Phys. Rev. Lett. **91** (2003) 112501.
- [11] G. Garbarino, A. Parreño and A. Ramos, Phys. Rev. **C 69** (2004) 054603.

- [12] E. Bauer and F. Krmpotić, Nucl. Phys. **A 717** (2003) 217.
- [13] E. Bauer and F. Krmpotić, Nucl. Phys. **A 739** (2004) 109.
- [14] B. H. Kang et al., Phys. Rev. Lett. **96** (2006) 062301.
- [15] M. J. Kim et al., Phys. Lett. **B 641** (2006) 28.
- [16] E. Bauer, G. Garbarino, A. Parreño and A. Ramos, e-Print nucl-th/0602066.
- [17] E. Oset and L. L. Salcedo, Nucl. Phys. **A 443** (1985) 704.
- [18] E. Bauer, Nucl. Phys. **A 818** (2009) 174.
- [19] E. Bauer and G. Garbarino, Nucl. Phys. **A 828** (2009) 29.
- [20] D. Jido, E. Oset and J. E. Palomar, Nucl. Phys. **A 694** (2001) 525.
- [21] E. Bauer, Nucl. Phys. **A 796** (2007) 11.
- [22] A. Parreño, A. Ramos and C. Bennhold, Phys. Rev. **C 56** (1997) 339;
A. Parreño and A. Ramos, Phys. Rev. **C 65** (2002) 015204.
- [23] V. G. J. Stoks and Th. A. Rijken, Phys. Rev. **C 59** (1999) 3009; Th. A. Rijken, V. G. J. Stoks
and Y. Yamamoto, *ibid.* 59 (1999) 21.
- [24] R. Machleidt, K. Holinde and Ch. Elster; Phys. Rep. **149** (1987) 1.
- [25] M. B. Barbaro, A. De Pace, T. W. Donnelly and A. Molinari, Nucl. Phys. **A 596** (1996) 553.
- [26] M. Kim et al., Phys. Rev. Lett. **103**, 182502 (2009).
- [27] M. Agnello et al., e-Print: arXiv:0910.4939 [nucl-ex].
- [28] W. Cassing et al., Eur. Phys. J. **A 16**, 549 (2003).
- [29] Y. Sato et al., Phys. Rev. **C 71**, 025203 (2005).
- [30] H. Outa, contributed talk at the PANIC08 conference, Eilat (Israel), November 9–14, 2008;
H. Outa et al., Nucl. Phys. **A 754** (2005) 157c.
- [31] M. Agnello et al., Phys. Lett. **B 622** (2005) 35; Nucl. Phys. **A 804** (2008) 151.
- [32] T. Nagae, Nucl. Phys. **A 754** (2005) 443c; Nucl. Phys. **A 805** (2008) 486c.
- [33] S. Ajimura et al., *Exclusive study on the ΛN weak interaction in $A = 4$ Λ hypernuclei*, Letter of
intent for an experiment (E22) at J-PARC (2007); H. Bhang et al., *Coincidence measurement
of the weak decay of $^{12}_{\Lambda}C$ and the three-body weak interaction process*, Letter of intent for an
experiment (E18) at J-PARC (2006).
- [34] T. Fukuda et al., Nucl. Phys. **A 790** (2007) 161c.
- [35] Note that an analogous inequality exists between Γ_n/Γ_p and the ratio between the total
number of emitted neutrons and protons, N_n/N_p [11]. For the present discussion any of these

two expressions is suitable.

(a)



(b)

